Rossi, C.; Villalaín, J.J.; Lozano, R.P.; Hellstrom, J.Paleo-watertable definition using cave ferromanganese stromatolites and associated cave-wall notches (Sierra de Arnero, Spain). Geomorphology. 261, pp. 57 - 75. 2016.

Paleo-water table definition using cave ferromanganese stromatolites and associated cave-wall notches (Sierra de Arnero, Spain)

By Carlos Rossi[1], Juan J. Villalaín[2], Rafael P. Lozano[3], and John Hellstrom[4]

[1] Dpt. Petrología y Geoquímica, Facultad de Ciencias Geológicas, Universidad Complutense, 28040 Madrid, Spain. crossi@geo.ucm.es
[2] Dpt. Física, E. Politécnica Superior, Universidad de Burgos, 09006 Burgos, Spain
[3] Museo Geominero, IGME. Ríos Rosas 23, Madrid 28003, Spain.
[4] School of Earth Sciences, the University of Melbourne, Victoria 3010, Australia

Abstract

The steeply-dipping-dolostone-hosted caves of the Sierra de Arnero (N Spain) contain low-gradient relict canyons with up to ten mapped levels of ferromanganese stromatolites and associated wall notches in a vertical range of 85 m, the highest occurring ~460 m above base level. Despite a plausible speleogenetic contribution related to pyrite oxidation, and irregular cave wall mesomorphologies suggestive of hypogenic speleogenesis, the Arnero relict caves are dominantly epigenic as indicated by the conduit pattern and the abundant allogenic sediments. Allogenic input declined over time due to a piracy-related decrease in the drainage area of allogenic streams, explaining the large size of the relict Arnero caves relative to the present-day outcrop of the karstified carbonates. Allogenic sediment input also explains the observed change from water-table canyons to phreatic conduits in the paleo-downstream direction. Stromatolites and associated notches arguably formed in cave-stream passages at the water table. The best-defined paleo-water tables show an overall slope of 1.7º, consistent with the present-day relief of the water table, with higher-slope segments caused by minor barriers related to sulfide mineralization. The formation of ferromanganese stromatolites at the water table favored wall notching by the combined effect of enhanced acidity by Mn-Fe oxidation and shielding of cave floors against erosion by the stromatolites themselves. The presence of abrasive clastic sediments further contributed to notch formation by preventing erosion of passage floors and promoting lateral mechanical erosion. The irregular wallrock erosional forms of Arnero caves are related partly to paragenesis and partly to the porous nature of the host dolostones, which favored intercrystalline irregular dissolution near passage walls, generating friable halos. Subsequent mechanical erosion further contributed to generate irregular forms and spongeworks. The dolostone porosity also explains the paradox that virtually all cave development in Arnero is focused on dolostone despite being much less soluble than adjacent limestone. U-series dating of carbonate speleothems and paleomagnetic data from ferromanganese stromatolites and clastic sediments indicate that the paleo-water tables recorded ~320 m above the present-day water table formed during the Matuyama Chron but prior to ~1.5 Ma, implying a long-term rate of base level lowering of ~125 to ~213 m per Ma. To our knowledge, this is the first attempt of paleomagnetic dating of cave ferromanganese deposits. Ferromanganese stromatolites are excellent geomagnetic recorders and offer a direct way to delineate and date paleo-water tables, especially in caves developed in dolostone.

Keywords: speleogenesis, karst, cave notches, paleo-water table, cave stromatolites, paleomagnetism, U-series dating, Sierra de Arnero.

1. Introduction

Relict caves are useful to trace the evolution of landscapes because they can record the elevation of ancient water tables, which in many karst areas are controlled by fluvial base levels. Therefore, mapping and dating such caves inform about the incision rates of valleys (e.g. Farrant et al., 1995; Granger et al., 2001; Stock et al., 2004; Polyak et al., 2008). Other possible indicators of incision rates such as river terraces or moraine deposits are more difficult to date

and more prone to be eliminated by erosion than caves, which can survive for millions of years due to the high resistance to erosion of most carbonate rocks.

Delineating paleo-water tables from elevations of relict caves is not straightforward. Water-table caves are obviously ideal for that task but unfortunately they are relatively uncommon (Gabrovšek et al., 2014): karst caves also form bellow (phreatic caves) and above (vadose caves) the water table. Batiphreatic caves for instance can form up to several hundred meters below the water table (Ford and Williams, 2007), and vadose caves can form up to 2 km above the water table in alpine regions (e.g. Rossi, 2004). Still, during periods of static base level, the main active cave conduits tend to cluster at similar elevations, resulting in a distinct cave "level" formed by water-table and/or shallow phreatic passages (Ford and Williams, 2007). In the latter case, the contemporary water table is defined where passage morphologies change from vadose to phreatic (Palmer, 1989, 1991). The paleo-water tables so defined are typically very low-relief (Palmer, 1989, Häuselmann et al., 2007), reflecting the high permeability of karst aquifers.

As surface rivers incise their valleys, the corresponding base-level fall induces the abandonment of water-table and/or shallow-phreatic conduits, creating new levels at lower elevations (Ford and Williams, 2007). However, processes such as glacial activity in the river headwaters may result in valley aggradation and subsequent base-level rise, inducing flooding and sediment filling of caves previously located near the water table. However, in most continental areas erosion dominates over episodic aggradation, resulting in net base-level lowering through time. Where valleys cut into karst rocks, these may develop cave levels that become progressively younger with decreasing elevation, creating an inverted stratigraphy comparable to that of river terraces (e.g. Sasowsky et al., 1995; Stock et al., 2005).

Both vadose entrenchment and breakdown can obscure the original cave passage profiles and morphologies, hindering the recognition of paleo-water tables. Vadose entrenchment of originally phreatic or water table passages may occur during base-level lowering, creating canyons whose floors may evolve into water-table passages (Gabrovšek et al., 2014). Also, even if a cave level becomes initially abandoned during base-level lowering, the corresponding passages may be captured and incised at any later time by vadose streams. Furthermore, not every low-gradient passage forms at the water table, and the mere presence of cave levels does not warrant a water-table control since levels may respond to lithological perching (Palmer, 1989). Therefore the use of caves as paleo-base level markers may benefit from developing reliable criteria for paleo-water table recognition in relict caves.

Sub-horizontal erosional notches formed in cave walls may define rather precisely the position of the contemporary water table and survive collapse and vadose entrenchment (Farrant and Smart, 2011). Such notches are particularly unequivocal as paleo-water table markers where the dip of beds and fractures is relatively steep, thus precluding a notch origin related to lithological controls. However, only certain caves develop notches, with allogenic sediment supply and aggradation of cave stream beds favoring their development (Farrant et al., 1995). However alluvial notches can also form in vadose caves related to upstrean alluvial sedimentation or ponding caused by local obstructions of cave streams (Farrant and Smart, 2011), therefore their presence does not guarantee a water-table origin.

El Soplao Cave (Sierra de Arnero, Spain) contains low-gradient relict passages with wall notches, detrital sediments and ferromanganese stromatolites, some of the latter having a minimum age of ~1±0.25 ma based on U-U dating of stalagmites (Rossi et al., 2010). Since the cave is developed in steeply dipping dolostones, a water-table control on the formation of both notches and stromatolites is likely. If so, ferromanganese stromatolites could represent an additional criterion for paleo-water table delineation in relict caves. In this paper, the previous suggestion by Rossi et al. (2010) that manganese stromatolites in El Soplao could cave formed at paleo-water tables is re-examined in the light of new data. We test that hypothesis by mapping notches and stromatolites, and studying passage morphologies and patterns, across the entire cave system including the previously un-examined eastern half of El Soplao and other closely related caves (Torca Ancha and Juñoso). We also analyze the role of detrital sediments and bed-rock lithology and porosity on speleogenesis and passage morphologies, explore the role of manganese oxidation reactions on chemical speleogenesis, and provide additional age

constrains of the inferred paleo-water tables based on new U-series data from carbonate speleothems and especially on the paleomagnetic analysis of detrital sediments and stromatolites. To our knowledge, the paleomagnetic dating of cave ferromanganese deposits has never been attempted before. If ferromanganese stromatolites do form at the water table, their dating offers a new and direct way to date paleo-water tables and derive rates of base-level lowering.

2. Geological and speleological Setting

The Sierra de Arnero (maximum elevation: 683 m asl) is located in the northern watershed of the Cantabrian Mountains of Northern Spain (Fig 1A). These mountains represent the western extension of the Pyrenees, an alpine chain resulting from the convergence of the Iberian and Eurasian plates. The uplift of the Cantabrian Mountains is related to crustal thickening linked to incipient Eocene to Miocene subduction (Álvarez-Marrón et al., 1997; Tavani, 2012).

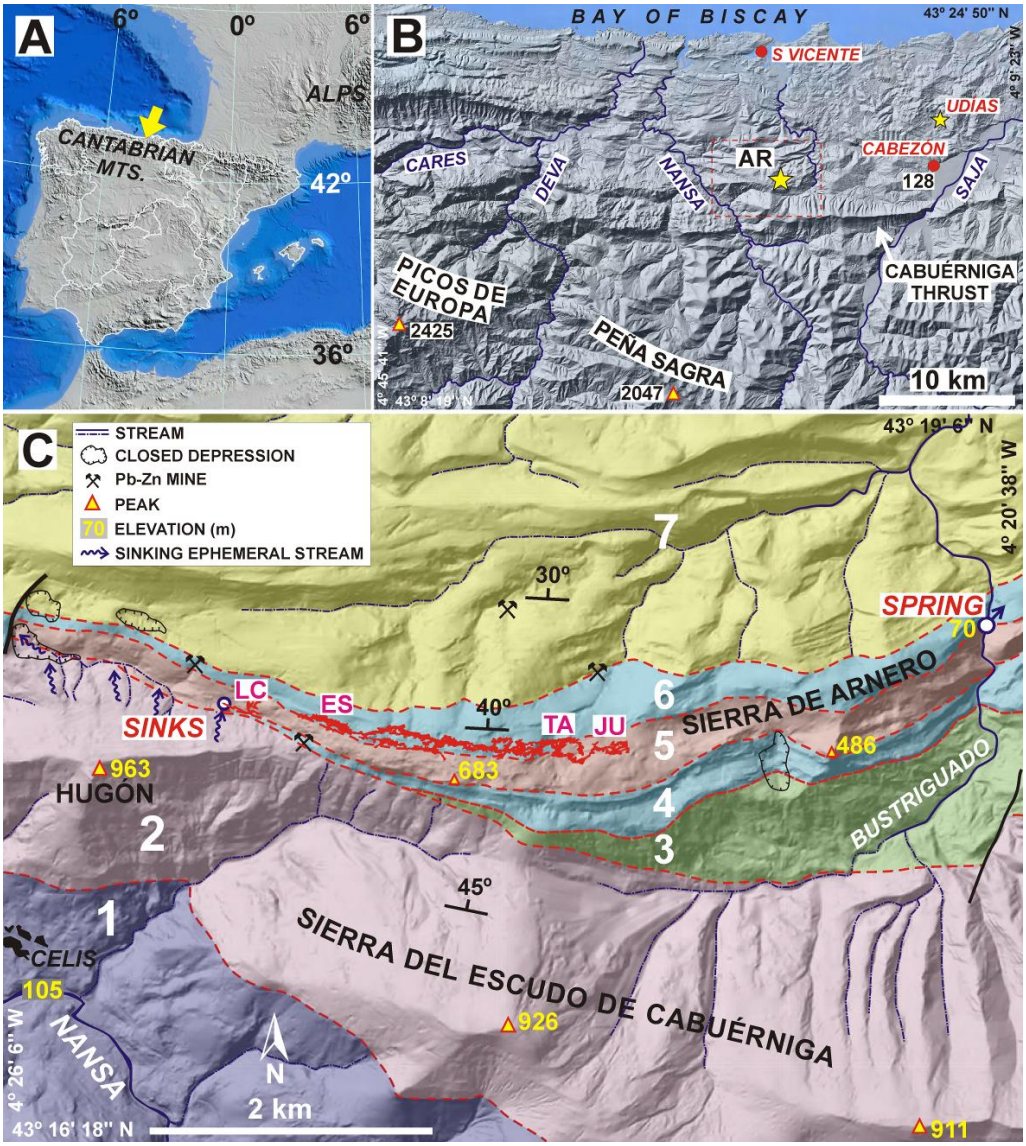

Fig. 1A: Location map of studied area (arrow). B: Map showing the location of the Sierra de Arnero (AR), major rivers, and other sites mentioned in text. C. Geological map of the Sierra de Arnero, showing the main caves (LC: La Cuerre; ES: El Soplao; TA: Torca Ancha; JU: Torca Juñoso). 1: Carboniferous; 2: Buntsandstein (Triassic sandstone and conglomerate). 3: Pre-Aptian siliciclastics; 4: Early Aptian limestones and marls; 5: Late Aptian dolostone (Reocín Fm); 6. Late Aptian limestones and marls (Reocín Fm); 7: Albian to Cenomanian siliciclastics and carbonates.

Near the Sierra de Arnero, surface elevations increase from sea level to more than 2 km in relatively short distances (20-30 km: Fig. 1B). The highest elevations are in the Picos de Europa (~2600 m) and Sierra de Peña Sagra (~2000 m) massifs, both of which developed extensive glaciers during Quaternary glacial periods (Serrano et al., 2013). The major north-flowing rivers are deeply incised creating spectacular gorges, especially in the Picos de Europa where they can reach up 1.5 km in depth. Those gorges generally maintain low longitudinal gradients, suggesting that fluvial incision has kept pace with uplift (Smart, 1986).

The Sierra de Arnero is mainly formed by Aptian to Albian carbonates and siliciclastics, dipping ~20º to ~50º to the north, and onlaping the Triassic Buntsandstein sandstones of the Sierra del Escudo de Cabuérniga (maximum elevation ~1000 m) (Fig. 1C). This Sierra represents a prominent E-W thrust unit which is dissected by several low-gradient, north-flowing rivers (Fig 1B). The Sierra de Arnero is located between two of these rivers: Nansa (to the west) and Bustriguado (to the east) (Fig 1B,C).

The caves of the Sierra de Arnero are developed in carbonates of the late Aptian Reocín formation, which dips ~40º to the north and shows a notable thickness variation, from ~400 m in the east (Bustriguado valley) to ~80 m in the west (Nansa valley) (Najarro et al., 2011). It consists of massive mesocrystalline dolostones sandwiched between two intervals of limestone with subordinate marls. The dolostone interval is of prime importance for speleogenesis since it contains all the major caves known in the Sierra de Arnero. Its thickness varies from ~140 m in the Bustriguado valley to ~40 m near the entrance to El Soplao cave (Najarro et al., 2011), being absent in the westernmost part of the Sierra.

The Reocín dolostones still retain matrix porosity (intercrystalline, moldic, and vuggy), part of which is lined by dolomite and calcite cements. In surface outcrop, weathering creates a characteristic spongework-like pattern and orange colors caused by the oxidation of ferrous iron released by dissolving ferroan dolomites. The dolostones host a Mississippi-valley-type mineralization, intensively mined from 1857 to 1978. Lead, zinc, and to a lesser extent iron sulfides filled partially collapsed paleokarst caves developed along the dip of the beds (Tornos and Velasco, 2011). Adjacent to the sulfide bodies, the dolostone matrix porosity is largely cemented by sulfides and dolomite. Three main sulfide-filled paleocave system were mined in the sierra de Arnero, two of them intercepted in sections of El Soplao cave (Fig 2B). The supergene oxidation zone of the sulfides is mainly formed by zinc and lead carbonates and extends from the surface to ~480 m asl (Fig. 2B).

The Reocín Formation represents the main aquifer of the Sierra de Arnero. The main spring is located at ~70 m asl in the Bustriguado valley (Fig. 1C), where groundwater discharges diffusely through the alluvium at rates from 0.03 to 0.12 m3/s (Meléndez and Rodríguez, 2011). That spring represents the base level for cave development in the Sierra. Present-day recharge is essentially autogenic by diffuse infiltration through the epikarst, with a fraction of allogenic recharge via intermittent streams that drain the Triassic sandstone outcrops of mount Hugon northern slope and sink at the sandstone-dolostone contact (Fig. 1C).

The main cave in the sierra (El Soplao) was discovered by accident in 1908 while excavating a tunnel in the Isidra mine (García et al., 2007). Other major caves of the Sierra are La Cuerre, Torca Ancha and Juñoso (Fig. 1C). Neither of these caves are physically connected to El Soplao through natural cave passages, but they are obviously part of the same cave system (Fig. 2), which contains 22 km of surveyed passages in 220 m of vertical relief (González, 2011). These are modest figures compared to the vast and deep limestone cave systems of nearby areas such as the Picos the Europa (Rossi, 2004) or eastern Cantabria, where at least three caves exceed 100 km in surveyed length. However, El Soplao cave is remarkable for the presence of well developed low-gradient relict passages, unusual erosional morphologies, and especially ferromanganese stromatolites containing exceptionally well preserved Mn-oxidizing bacteria (Lozano and Rossi, 2012) and zaccagnaite-3R, a new mineral polytype of the hydrotalcite group (Lozano et al., 2012). Due to the abundance of aragonite helictites and other carbonate speleothems (Delgado Huertas et al., 2010; Gázquez et al., 2012), the western sector of El Soplao was developed as a show cave. Access to parts of the central sector of the cave is facilitated by an extensive network of abandoned mine passages totaling at least 25.6 km (González, 2011; Fig 2). The westernmost part of the cave was not intercepted by mining

and was explored in relatively recent times. Despite exploration efforts, El Soplao has no known natural access from the surface. By contrast, both Torca Ancha and Torca Juñoso have natural entrances consisting of relict phreatic passages intercepted by recent erosion (Fig. 2).

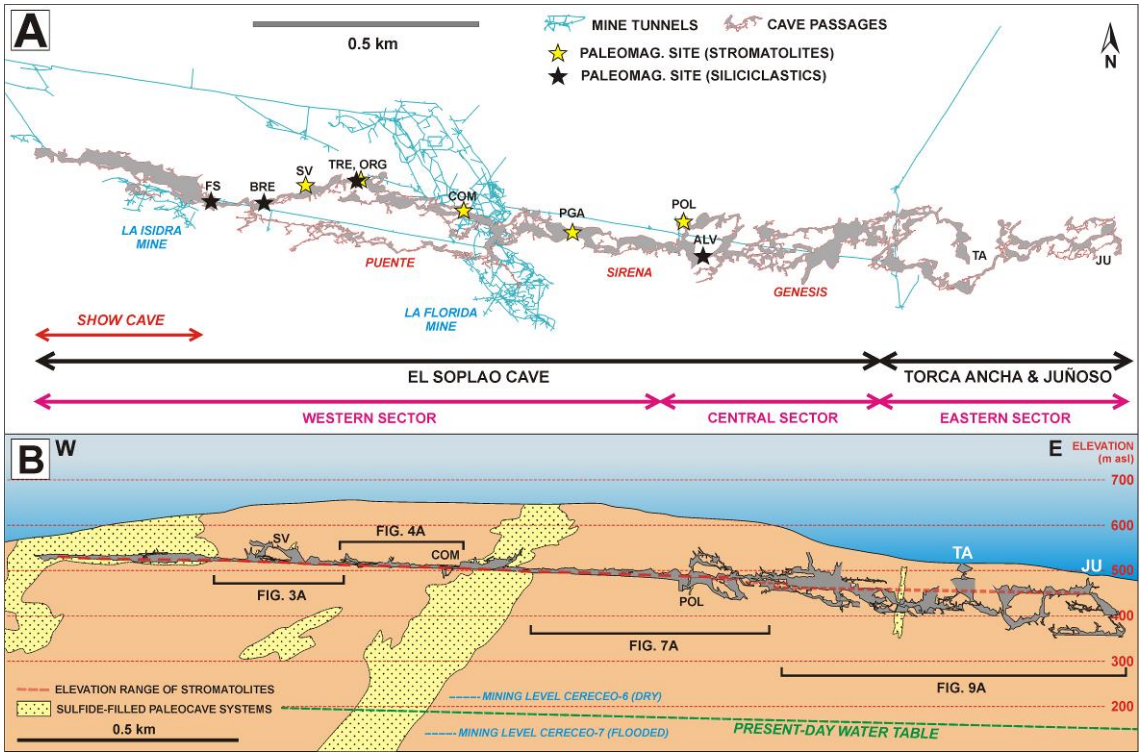

Fig. 2. A: plan view of El Soplao, Torca Ancha (TA) and Juñoso (JU) caves, showing the paleomagnetic sample sites and the survey of abandoned mining galleries. B: E-W projected view of El Soplao-Torca Ancha-Juñoso cave system and the land surface, showing the main stromatolite assemblages and the location of the sulfide-filled paleocave systems. Some overlapping passages are omitted for clarity.

3. Methods

Survey data was available from Zalama Multiservicios (Ramales, Cantabria). Distances, inclinations and azimuths between stations were measured with a DistoX laser meter equipped with tilt and azimuth sensors. Survey stations were located and marked on protuberances of cave walls, with station numbers labeled on removable cards. Passage dimensions at each station were measured with a laser meter. Average loop-closure error is 1.75%. Geomorphic features were mapped along most of the cave system including the relatively remote areas of western El Soplao, Torca Ancha and Juñoso, using prints of projected elevations of the survey line. A total of 73 detailed passage cross sections were drawn in situ, with distances and vertical angles of key geomorphic features to the nearest survey stations measured using a laser meter Disto D8.

Paleomagnetic sampling was performed on both detrital sediments and stromatolites to provide age constraints. For the detrital sediments, due to their unconsolidated nature we used a non-ferromagnetic metal cylinder with a built-in orientating system. The 1.6-cm-diameter (3.6 cm^3) samples were kept in cylindrical plastic boxes. In each of the 7 sampled sites, we intended to cover the vertical range exposed, with sample spacing ranging between ~5 and ~10 cm. 5 to 20 samples were taken from each site, totaling 56 samples spanning a vertical range of 95 m. Five detrital sediment sites are in the main relict canyon at elevations ranging from 496 to 512 m asl (sites POG, ORG, COM, PGA1 and PGA2: Fig. 2). Site SV represents an upper level phreatic tube (elevation: 553 m) and site POL is at a lower elevation (458 m) (Fig. 2). For the ferromanganese stromatolites, 2.5-cm-diameter cores were drilled with an electric drill at nine sites representing five stromatolite levels of the main relict canyon (5-10 samples per site, totaling 69 samples). Remanence measurements were performed with a 2G cryogenic superconducting magnetometer (755 DC SQUID) at the Burgos University. For the detrital sediment samples, we used stepwise alternating field (AF) demagnetization up to a peak field of

100 mT. Due to their plastic encapsulation, thermal demagnetization could not be performed in those samples. For the stromatolites, we used both stepwise AF and thermal demagnetization using a TD-48-SC oven. Three orthogonal components of isothermal remanent magnetization (IRM; 2 T, 0.4 T and 0.12 T, respectively) were induced in representative stromatolite samples and subsequently stepwise demagnetized following the method proposed by Lowrie (1990), in order to compare the coercivity and unblocking spectra of ferromagnetic phases.

Trim ends from 34 stromatolite plugs were vacuum impregnated with epoxy, thin sectioned, and the polished thin sections imaged under combined transmitted and reflected light using an Olympus BX51 petrographic microscope. The resulting images were used to evaluate the presence and abundance of replacive calcite, a common diagenetic alteration phase in ferromanganese stromatolites (Lozano and Rossi, 2012).

To determine composition and provenance, three sand samples were impregnated with epoxy resin, thin sectioned, imaged under cathodoluminescence, and their relative abundances of quartz, feldspar and dolomite clasts were counted digitally, in all cases following the methods detailed in Rossi and Alaminos (2014). Samples POG-7 and PLY-1 are from sands overlying stromatolites (ST3, ST6). Sample POS-1 represents sands interbedded with clays and silts sampled for paleomagnetism (POL site).

To constrain the age of the main relict canyon and their stromatolites, three stalagmites and one flowstone were retrieved for U-series dating. The speleothems were slabbed and scanned, and 19 sub-samples (~20 mg) were microdrilled from layers free of detrital material. Isotope ratios were measured in a Nu Instruments multicollector inductively coupled plasma mass spectrometer following the procedures of Hellstrom (2003). U-Th ages and initial 234U/238U activity ratios were calculated using the Monte Carlo method implemented in Isoplot (Ludwig 1999) assuming an initial 230Th/232Th activity ratio of 1.5±1.5.

4. Results

4.1. Passage pattern, morphologies and deposits

Most cave passages in the Sierra de Arnero are developed along the strike of the beds (Fig. 2A), and virtually all are contained in the Reocín dolostones. Based on predominant passage morphology, the cave system is subdivided into three sectors: western, central and eastern (Fig. 2).

4.1.1 Western sector

This sector mainly consists of a low-gradient relict canyon (Fig. 2B) guided by looping phreatic conduits (Fig. 3A). Additional relict phreatic tubes are present at different elevations above the ceiling of the canyon (Fig. 3A), and are partly filled with laminated clay (SV site). In these upper-level phreatic tubes, vadose trenches are sparse. Canyon walls are commonly inclined following the statal dip (Fig. 3). The canyon contains four levels of ferromanganese stromatolites (described in detail in Rossi et al., 2010), named ST1 to ST4 in order of decreasing elevation, and associated subhorizontal wall notches (Fig. 3B). ST1 and ST4 are relatively discontinuous and their corresponding notches moderately developed (Fig. 3B). In the lower part of the canyon, ST3 and ST4 are more continuous and their associated notches very well developed (Fig. 3C,D), locally extending up to ~15 m into canyon walls. Because the direction of notch widening is generally perpendicular to the strike of the beds, the collapse of wedge-like blocks of dolostone is common where the notch intercepts a bedding plane (Fig. 3E,F). In some sectors of the main canyon (such in the show-cave path: Fig. 2A), breakdown has almost obliterated passage morphology, but remnants of notches and stromatolites are still present in canyon walls. Where the relict canyon meets the main sulfide-bearing paleocave system (Fig. 2B), passage morphology is obscured by mining. Elsewhere, the canyon floor is covered by siliciclastic sediments (Fig. 3C) and stromatolites (Fig. 4A), so that the erosional bedrock base cannot be observed.

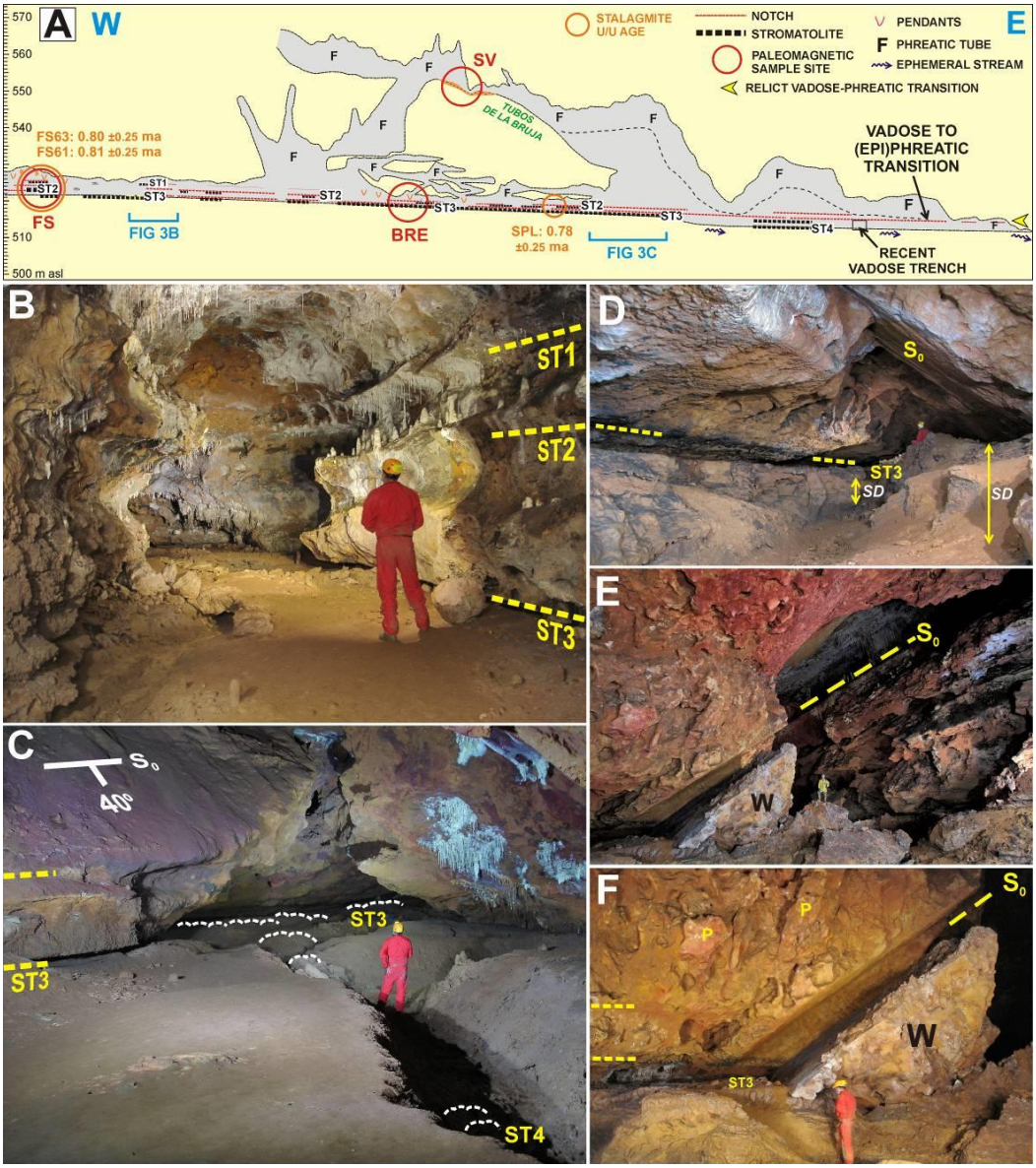

Fig 3: A: Projected elevation of a upstream section of the main relict canyon (location in Fig. 2B), showing the distribution of stromatolites, notches, and sample sites. B: Typical view of notch levels (location in A). The lowermost notch contains stromatolites, partly covered by sediments and a miner's path. C: Subhorizontal notches cut into dolostone beds dipping 40º (location in A). Stromatolites are largely buried under siliciclastics, but some are uncovered by recent vadose incision. D: Relatively thin and wide notch. Passage floor is covered by stromatolites (ST3) and siliciclastics (SD). The ceiling is partially collapsed revealing a bedding plane (S_0). E: Breakdown wedge (W) formed at the intersection of a notch and a bedding plane (S_0), which is also guiding the canyon and its phreatic ceiling. Photo by Roberto F. García - www.espeleofoto.com. F: Detail of E, showing extensive paragenetic modification of canyon walls (pendants: P).

Although locally the stromatolite levels seem vertically juxtaposed (Fig. 4B), we have not observed stromatolites from a particular level overlying stromatolites of the next level. Instead, the stromatolites overlie either clastic sediment or bedrock. Each stromatolite level seems to be confined to a specific notch, where mushroom-like stromatolitic domes are interbedded with quartzose gravel and sand (Fig. 4C), forming a sequence of terraces whose ages are inferred to become younger downwards.

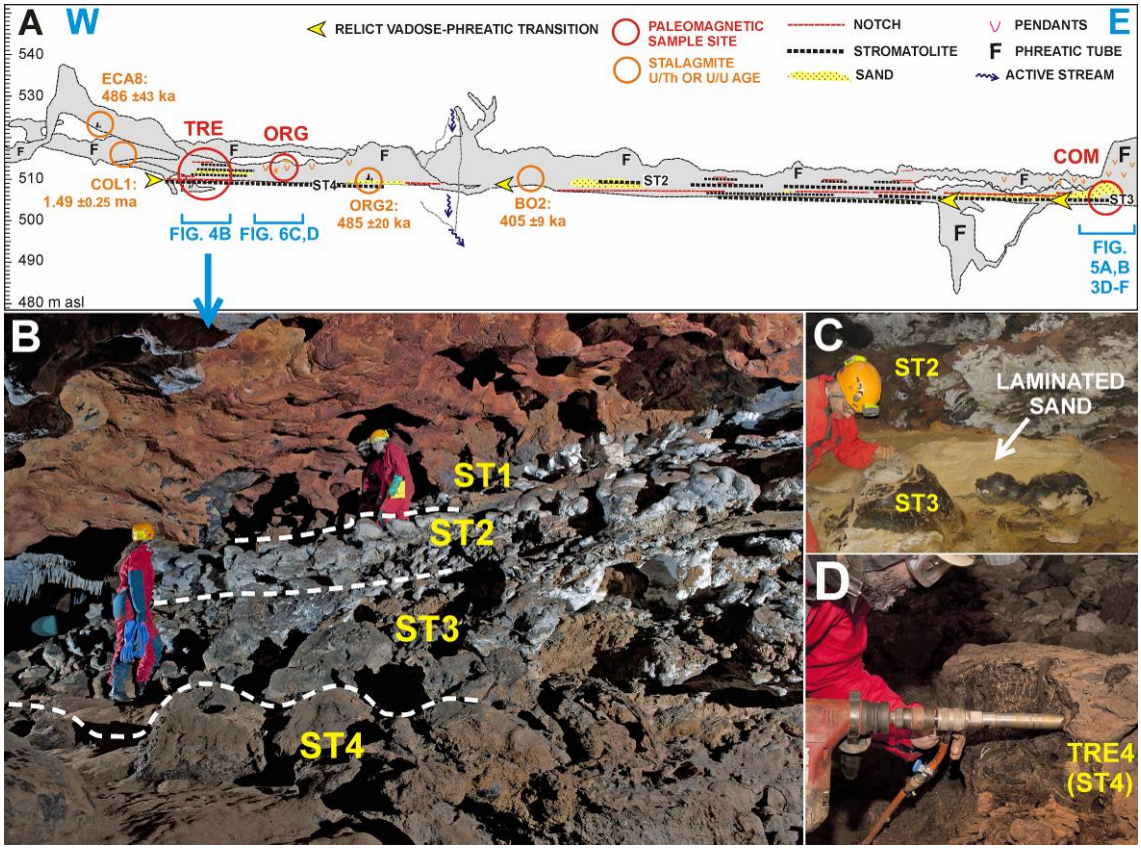

Fig. 4. A: Projected elevation of part of the main relict canyon (location in Fig. 2B), showing the distribution of stromatolites, notches, and sample sites. B to D: Paleomagnetic sampling site TRE, where stromatolite levels ST1 to ST4 are preserved in the same passage (B: photo by Alberto Uyarra).

A fining-upwards sequence of cross-laminated sand and minor silt usually covers the stromatolites or their associated notches (Fig. 5A,B). This sandy sequence covers the canyon floor in most of the western sector, where is commonly capped by vadose carbonate speleothems. Therefore, the stromatolites are only observed where their sand cover has been removed either by recent incision by ephemeral streams or by mine workings. The sands can locally reach up to 2.5 m in thickness and appear to postdate the four stromatolite levels. The oldest siliciclastic sediment preserved in the relict canyon is represented by reddish clay, which is locally exposed in the upper part of the canyon predating ST1 (Fig 5C), in pockets in the canyon walls and ceilings (Fig. 6), or in the lower part of the canyon (Fig. 5B).

Paragenetic modification of the walls and ceilings of the relict canyon is widespread: residual rock pillars (i.e. pendants) between anastomotic, sinuous half-tubes are very common (Figs. 3F, 5A), with individual pendants locally reaching up to 2 m in height (Fig. 6A-B). The absence of scallops on cave walls or ceilings is notable. The dolomitic bedrock adjacent to cave walls is commonly corroded at microscale, resulting in a halo of more porous, friable dolostone of centimetric thickness. Remnants of reddish clay are commonly preserved between pendants (Fig. 5B) and in pockets in passage ceilings and walls (Fig 5C,D), evidencing a phase of phreatic clay sedimentation subsequently eroded prior or during the formation of notches and stromatolites.

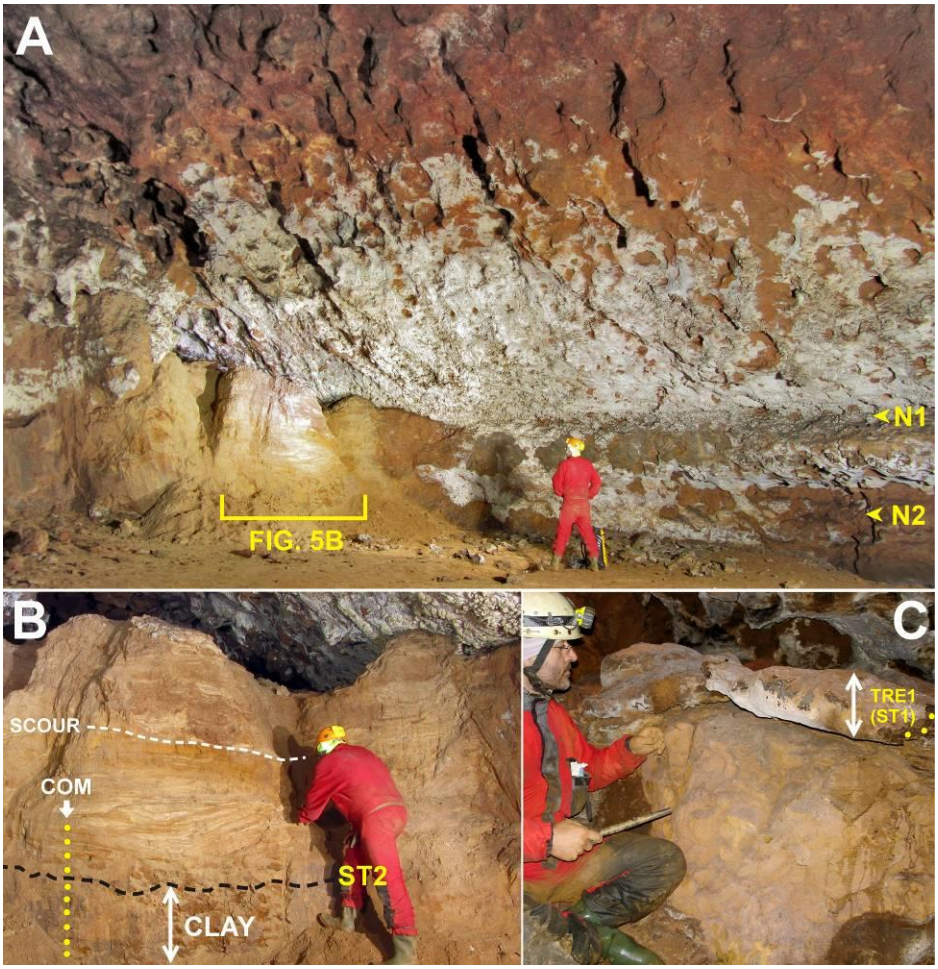

Fig. 5. A: Paragenetic modification of canyon walls. Pendants are developed between complex sinuous half-tubes. Notches N1 and N2 correspond to stromatolites ST1 and ST2, respectively. The lower part of the canyon is partially filled with clay and cross laminated sand. B: Detail of A, corresponding to paleomagnetic site COM. The reversed-polarity basal clay is capped by an erosive surface, an incipient stromatolite (ST2) and a fining-upwards sequence of medium to fine-grained sand containing scour and fill structures. C: Detailed view of paleomagnetic sample site TRE1, where stromatolite ST1 overlies clay.

Few phreatic tubes are known below the level of the main relict canyon floor (e.g. Fig. 4A), possibly because they are filled with sediment. In fact, where such conduits are accessible they commonly contain abundant clay. Because those phreatic tubes are preserved without significant vadose incision, the points where they intersect the low-gradient canyon floor represent vadose (or epiphreatic) to phreatic transitions (Fig. 4A).

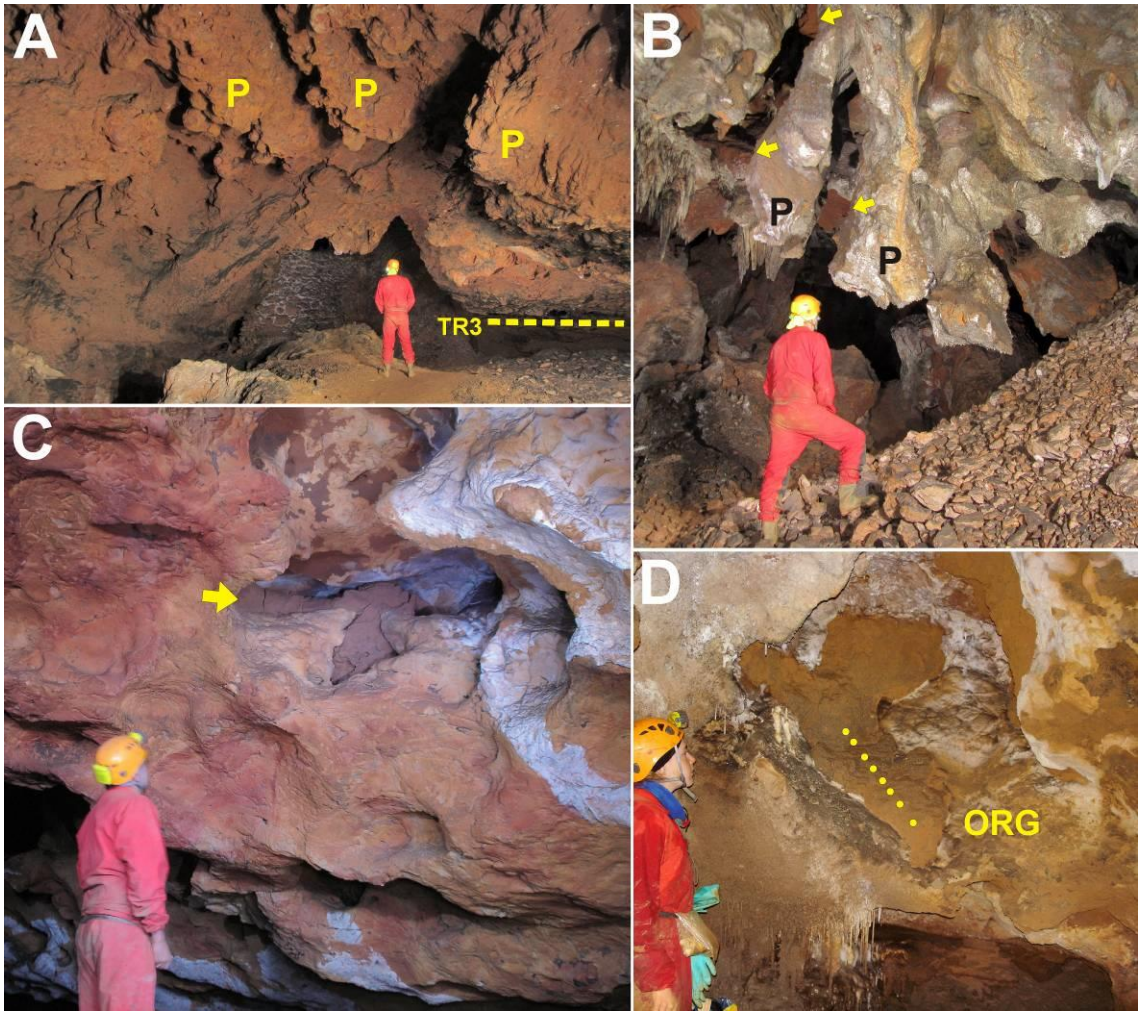

Fig. 6. A,B: Prominent pendants (P), some exceeding 2 m in height, developed in the ceiling of the main canyon and locally preserving remnants of reddish clay between the pillars. C: Pocket of reddish clay (arrow) preserved in the canyon walls (location in Fig. 4A). D: Similar to C, showing the location of samples of paleomagnetic site ORG.

An additional low-gradient relict canyon (Puente, Fig. 2A) is developed to the south of the main canyon and at virtually the same elevations. It also contains notches and abundant siliciclastic sediments, and apparently represents an inlet of the main canyon.

4.1.2 Central sector

To the east, the main relict canyon grades into a large looping phreatic tube developed at elevations up to 50 m below the canyon level (Fig. 7A,B,C). That tube intersects the low-gradient canyon in two successive points, representing outstanding examples of vadose to phreatic transitions. Further downstream, the low-gradient canyon disappears completely, being replaced by an assemblage of phreatic conduits (Perro, Fig. 7A) partly developed at slightly lower elevations than the canyon. The large looping phreatic tube is floored by detrital sediments in its upstream, western part (Fig. 7B). More downstream, the tube is essentially free of siliciclastics (Fig. 7C). The large looping phreatic system exploits a bedding plane or bedding-parallel fracture, and also extends up to 65 m above the level of the canyon (Fig. 7A). This upper part of the phreatic system was relict when the water table was at the level of the main low-gradient canyon.

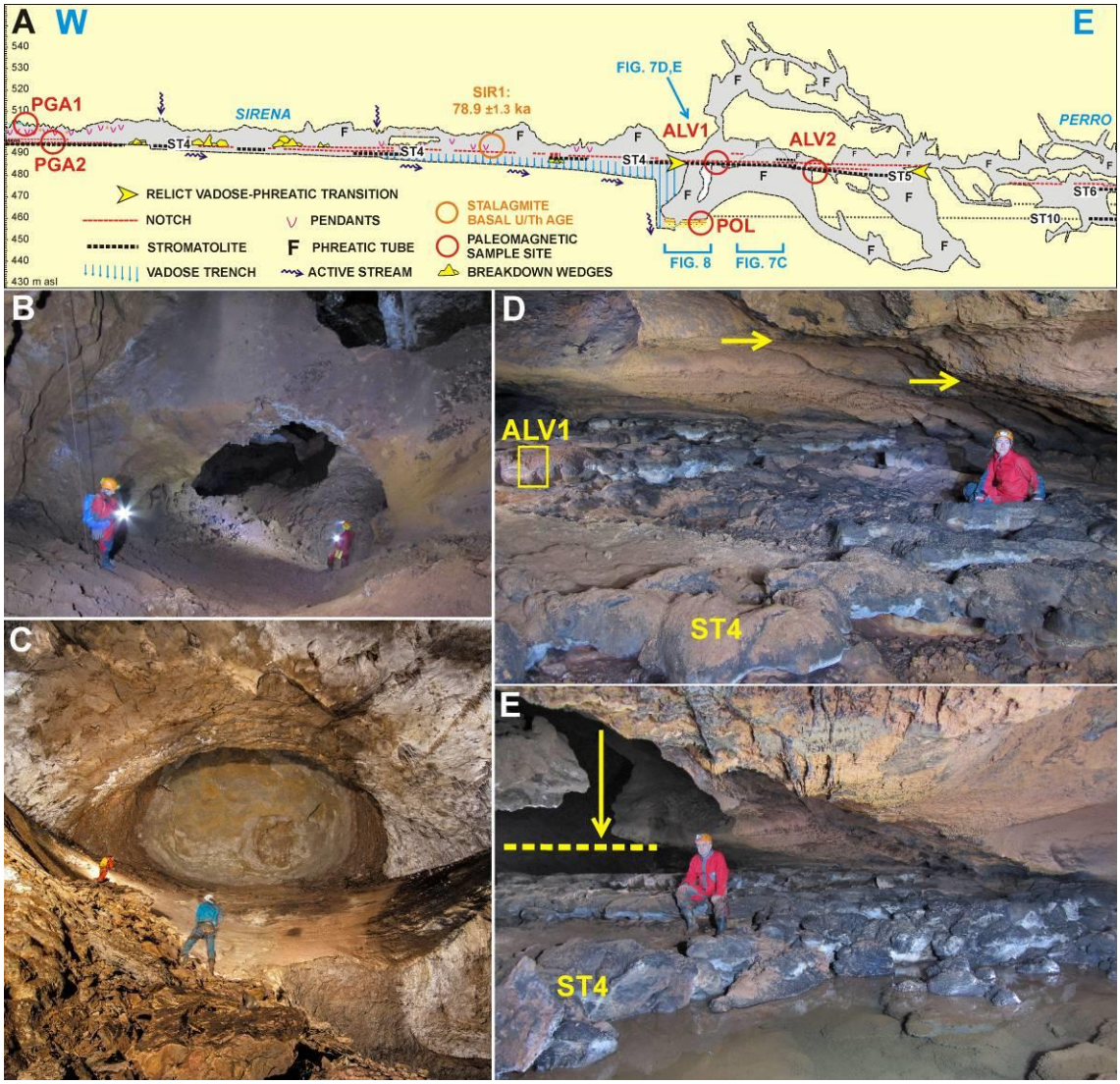

Fig. 7: A: W-E projected elevation of the transition between the western and central sectors, showing the location of paleomagnetic samples. B: Upstream portion of the large phreatic looping tube below the ALV sites, showing the abundant detrital sediment at the floor. C: Up-loop of the same phreatic tube, downstream of B. Photo by Anita Sobrino - www.espeleofoto.com. D-E: ALV-1 site. ST4 stromatolites are uncovered by sediment and thus exceptionally well exposed. Horizontal arrows point to moderately developed notches slightly above the stromatolite level, where passage widening is maximum. Vertical arrow indicates the direction of entrenchment in the canyon prior to notch/stromatolite formation.

In the segment of low-gradient canyon located between the two connections to the large looping tube (ALV sites; Fig. 7A), the ST4 stromatolites lack sand cover (Fig. 7D,E), making this sector probably the most spectacular exposure of cave stromatolites so far described. Locally, the stromatolites overlie notched dolostone bedrock with a characteristic spongework morphology. A branch of the large phreatic loop ends in a subhorizontal siliciclastic sediment plug with impressive mud cracks (site POL; Fig. 8). The top surface of the sediments is slightly below the level of a moderate notch covered by a ferromanganese crust (Fig. 8B) interpreted as a paleo-lake level, correlative to stromatolite level ST10 found more downstream (see below).

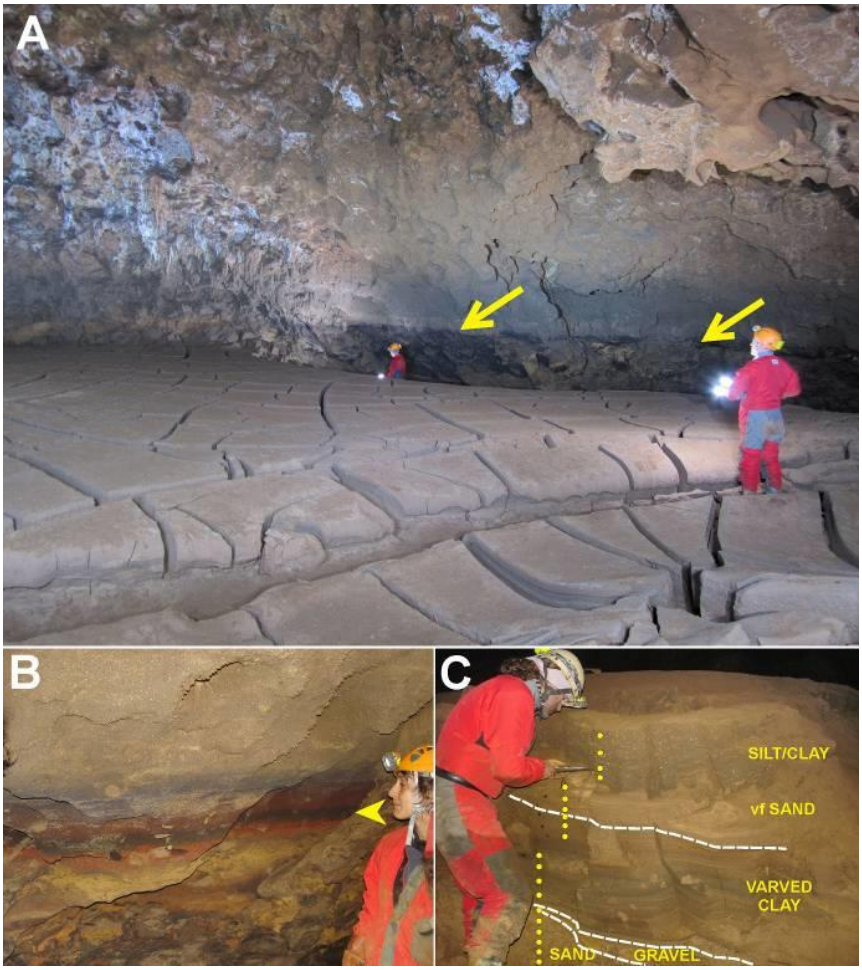

Fig. 8. Paleomagnetic sample site POL, where a large phreatic tube is filled with predominantly argillaceous, subhorizontal sediments with large mud cracks. A moderate horizontal notch (A, arrows) is covered by a ferromanganese crust (B, arrow) defining a paleolake level. The sediments mainly consist of finely laminated clay and silt (C), with sand and gravel in the base of the exposed sequence.

Downstream of the Perro phreatic assemblage (Fig. 7A), the relict canyon morphology is recovered (Genesis canyon: Fig. 9A), with a vertical extent larger than in the low-gradient canyon of the western sector. Genesis canyon contains four additional stromatolite levels (ST6 to ST10) with associated notches. Extensive breakdown by collapse of mega-wedges is related to the lowermost notch. Locally, some passages are developed in limestone, where notch levels are remarkably smoother, flatter, and better developed than in dolostone (Fig. 9B). In Genesis canyon, features correlative to level ST4 include a prominent notch and an epiphreatic conduit with incipient notching and rare stromatolite remnants (Cenital passage: Fig. 9A). At higher elevations, large looping phreatic tubes relatively free of clastic sediments are present. Below the floor of the Genesis Canyon, there is an additional system of phreatic tubes, relatively free of detrital sediments, and showing a characteristic spongework erosional morphology (Fig. 9C).

4.1.3 Eastern sector

This sector, represented by Torca Ancha and Juñoso caves, mainly consists of looping phreatic tubes (Fig. 9A), with rare low-gradient passages including a relict notched canyon with stromatolites at elevations correlative to level ST10 (Fig. 9A). Similar to the central sector, in the eastern sector detrital sediments are scarce. The lowermost passages are represented by a low-gradient, hydrologically active narrow vadose meandering canyon developed in limestone. The canyon floor is virtually devoid of clastic sediment, with well developed scallops on canyon walls (Fig. 9D). Although the stream has a low gradient and is limited by sumps, it is unlikely that it represents the present-day water table because the stream is still ~200 m above the lowest occurrence of unflooded mine passages (Fig. 2B).

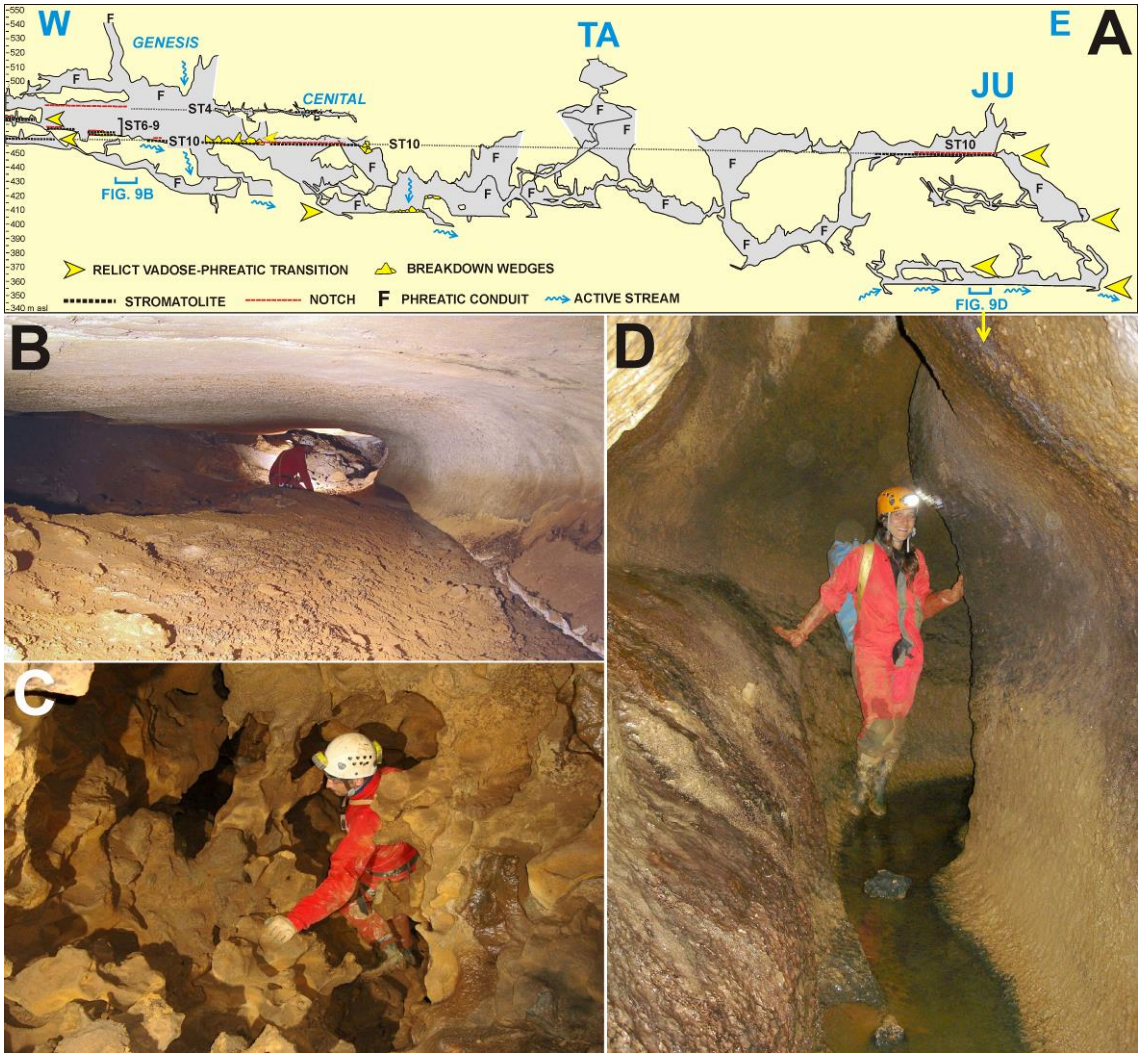

Fig. 9. A: W-E projected elevation of the transition between the central and eastern sectors, showing the location of entrances to Torca Ancha (TA) and Juñoso (JU) caves. B: Notch corresponding to stromatolite level ST6 developed in limestone, central sector. C: Spongework erosional morphology developed in a phreatic passage below the main canyon of the central sector. D: low-gradient active meandering canyon developed in limestone in Juñoso cave. Note the scallops and the absence of clastic sediments. Photos B and C by AER.

4.3 Correlation of stromatolite and notch levels across the cave system

We have mapped 10 stromatolite levels in a vertical range of 85 m, the highest occurring about 460 m above base level. The confidence of the stromatolite correlation is higher in the main relict canyon, where stromatolite levels (ST1 to ST4) and their associated notches can be followed over relatively long distances (Fig. 10). The prominent notches linked to ST3 and ST4 facilitated the correlation (Fig. 10). However, the continuity of both stromatolites and notches is interrupted where passage morphology changes from canyon to phreatic tube (e.g. Fig. 3A and 4A): the phreatic passages do not contain stromatolites or notches, probably because they formed below the level of the coeval canyon floor. Where the stromatolite levels are interrupted by changes in passage morphology or mine workings, the levels are correlated based on the distribution of notches and by extrapolating gradients from the sections where the stromatolite levels are more continuous.

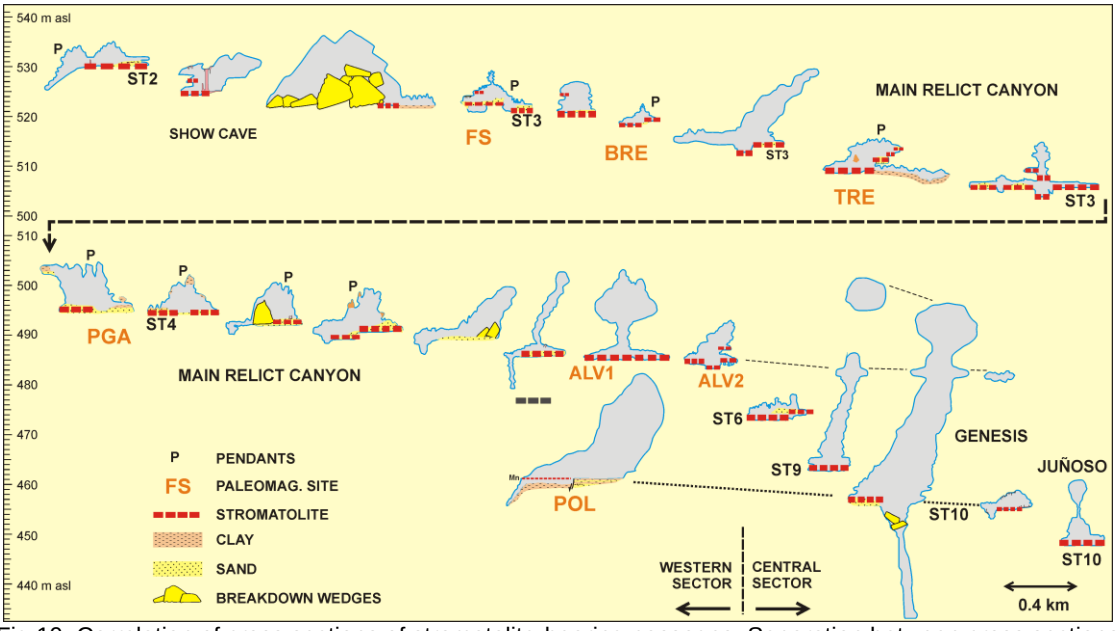

Fig 10: Correlation of cross sections of stromatolite-bearing passages. Separation between cross sections not to scale.

Predominant paleoflow in the cave system was to the east as indicated by the gradients of the relict canyons (Fig. 2B), notches and stromatolites (Fig. 3A and 10). Present-day flow of vadose streams captured by relict passages is also regularly toward the east (e.g. Fig. 9A). Overall, the gradient defined by the most extensive stromatolite assemblage (ST1 to ST4) is 1.7º to the east (Fig. 2B). In the four sections where that stromatolite assemblage is more continuous, measured gradients are, from west to east, 1º, 2.3º, 1.6º, and 1.7º.

4.4 Paleomagnetic results

The stromatolite samples present Natural Remanent Magnetization (NRM) intensities between 0.5 and 50 mA/m. Systematic demagnetization by both thermal and AF techniques (Fig. 11A-F) indicates that the NRM of most samples contains a low-unblocking-temperature (<250ºC) and low-coercivity (<10 mT) component, which is probably an unstable viscous overprint. After eliminating this component, a stable normal- or reversed-polarity component with maximum unblocking temperatures of about 550ºC is revealed (Fig. 11A,C). We consider this component the Characteristic Remanent Magnetization (ChRM), whose coercivity ranges from 10 to ~40 mT. In some samples, a fraction of higher coercivity with the same direction as the ChRM is observed in AF demagnetization diagrams (Fig. 11D,E). The maximum unblocking temperatures of the ChRM suggest that magnetite is the carrier of this component. The thermal demagnetization of three IRM components (Fig. 12), confirms that magnetite is the main ferromagnetic mineral: The low-coercivity phase (<0.12 T) shows a clear drop at an unblocking temperature of 550-575ºC. This experiment also reveals small amounts of hematite in the hard phase (Fig. 12B), responsible for the high coercivity fraction of the NRM. In some stromatolite samples, the ChRM can not be isolated because the NRM include several components and the low-coercivity phases dominate the magnetization (Fig. 11F). These samples commonly show signs of diagenetic alteration as revealed in thin section by the presence of solution vugs and replacive calcite containing minute inclusions of ferromanganese oxides.

The NRM intensity of the detrital sediments fluctuates between 0.5 and 100 mA/m. In many samples, AF demagnetization reveals two directional components (Fig. 11G-J): a viscous normal-polarity component removed at peak fields of 10 mT, and a medium-coercivity component (10-40 mT) showing both normal and reversed polarities depending on the sampling site. We interpret this component as the ChRM. In some samples, a high-coercivity phase still remains after cleaning at 100 mT. This phase generally has the same direction as the ChRM. In same sites, magnetization becomes negligible after peak fields of 10 mT hampering the isolation of the ChRM. Although the studied detrital-sediment sites mainly consist of clay and

silt, some sand samples were also analyzed. Sands regularly yielded inconsistent directional data probably due to the inadequate particle size of ferromagnetic minerals, and will not be considered further.

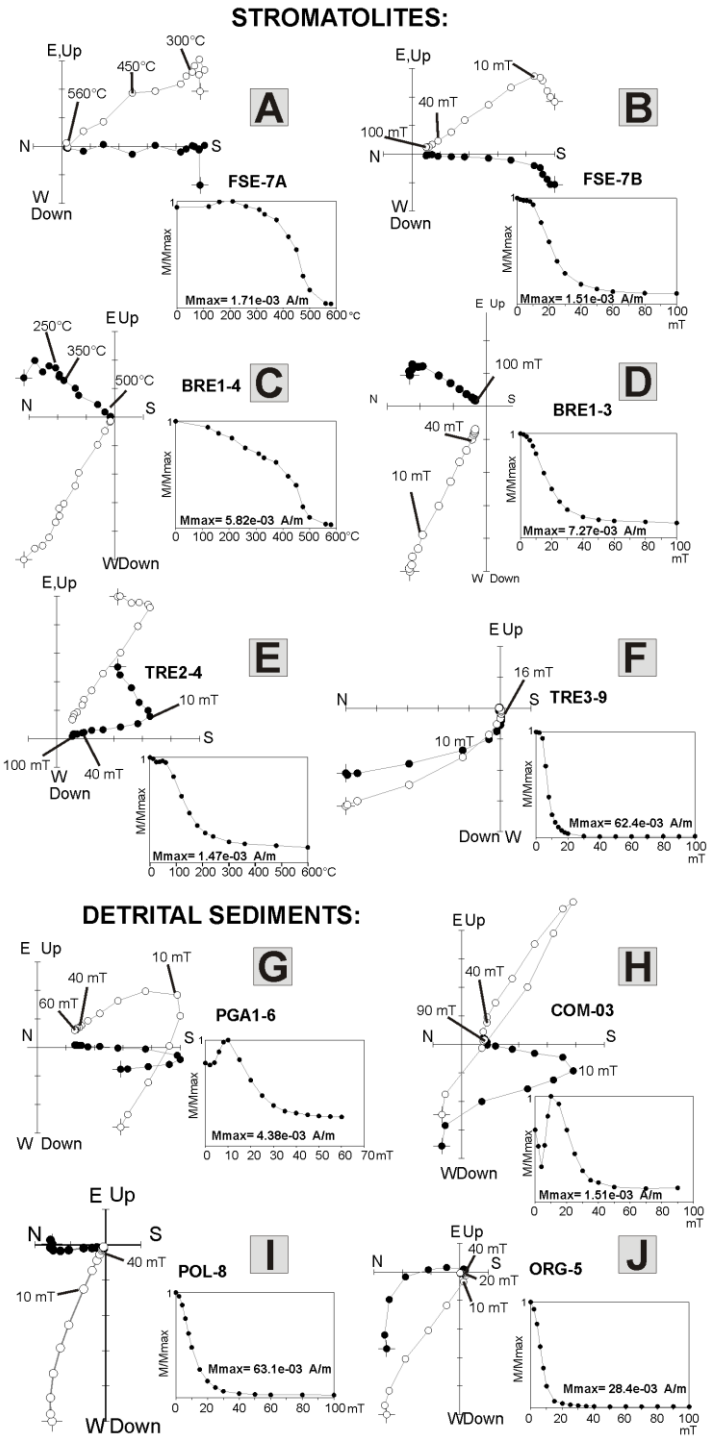

Fig. 11. Zijderveld proyections of representative samples in geographic coordinates (A-F: stromatolite; G-J: detrital sediments). Solid symbols indicate projections of vector end points onto the horizontal plane, and open symbols onto the vertical plane. The corresponding plot of the evolution of normalized NRM intensity (M/Mmax) during the thermal (A,C) and AF (B,D-J) demagnetization is also plotted. A and B: thermal and AF demagnetization of two stromatolite subsamples of the same core. The ChRM shows reversed polarity in A, B, E, G, and H, and normal polarity in C, D, and I.

In most samples (75 %), the ChRM show paleomagnetic directions consistent with the expected Earth's Magnetic Field, showing both reversed and normal polarities, with net predominance of the former. Some stromatolite samples show a stable ChRM component with anomalous

directions (Fig. 14B). Most of these samples present signs of diagenetic alteration as revealed in thin section. After excluding anomalous samples, mean directions of both normal and reversed stromatolite sample sets are antipodal. The statistical reversal test is positive at 95% confidence level with classification 'C' (McFadden & McElhinny, 1990). However, the detrital sediments present more dispersion and the reversal test is indeterminate. The 95% confidence intervals of the mean direction (after transpose all directions to normal polarity) of both stromatolites (D=0.4º; I=61.8º; α_{95}=7.9º) and detrital sediments (D=1.3º; I=47.9º; α_{95}=10.2º) contain the expected geomagnetic direction after averaging its secular variation. Therefore, the analyzed samples effectively record the geomagnetic field.

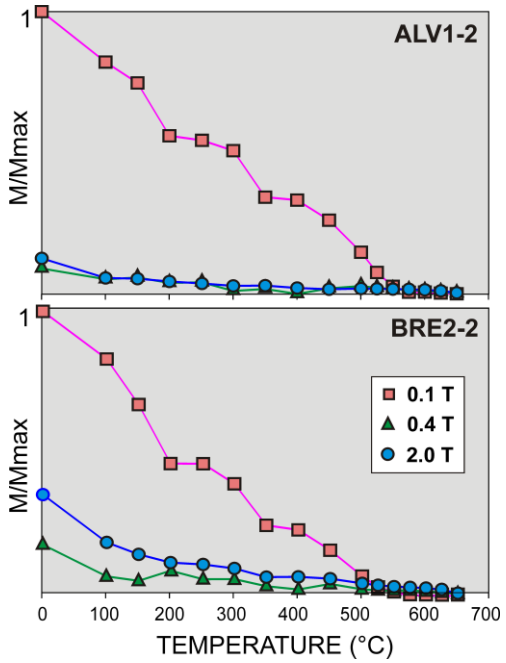

Fig. 12. Unblocking temperature spectra of three orthogonal IRM components of representative stromatolite samples.

4.2.1 ChRM directions in detrital sediments

At elevations above the level of the main relict canyon (SV site), the analyzed samples show reversed polarities (Fig. 13B). In the main relict canyon, all the detrital-sediment sites yielded reversed polarities (Fig. 13B), including clays associated to pendants near the canyon ceiling (PGA1 site), isolated clay pockets in canyon walls (ORG site: Fig. 6D), laminated clays predating ST2 (COM site: Fig. 5B), and laminated silts postdating ST4 (PGA2 site). Below the level of the main relict canyon (POL site), the analyzed samples show consistently normal polarities (Fig. 13B).

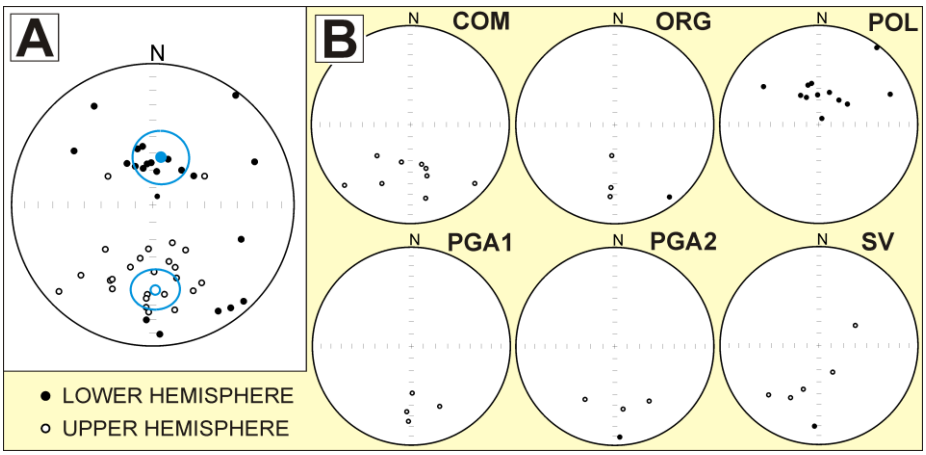

Fig. 13: Equal area stereographic projections of the ChRM directions for detrital-sediment samples (small circles). A: Directions for all samples, including means and 95% confidence areas of the normal-polarity and reversed-polarity populations. B: ChRM directions for individual sites.

4.2.2 ChRM directions in stromatolites

Most unaltered stromatolite samples from levels ST1 to ST4 have reversed polarity (sites FS, BRE, TRE1 to 4, and ALV1: Fig. 14). However, two stromatolites assigned to levels ST2 and ST4 also contain apparently unaltered samples showing normal polarity: in site BRE1 (ST2), unaltered samples yielded reversed polarities in the inner part of the stromatolite, and normal polarities in the outer part. Elsewhere, stromatolites assigned to ST2 (sites FS and TRE2) show consistently reversed polarities. In stromatolite TRE4, samples have normal polarity in the core and reversed polarity in the outer layers. Other unaltered stromatolite samples from ST4 sites have reversed polarity (site ALV1). All the samples from level ST5 (site ALV2) have normal polarity and show no visible signs of diagenetic alteration.

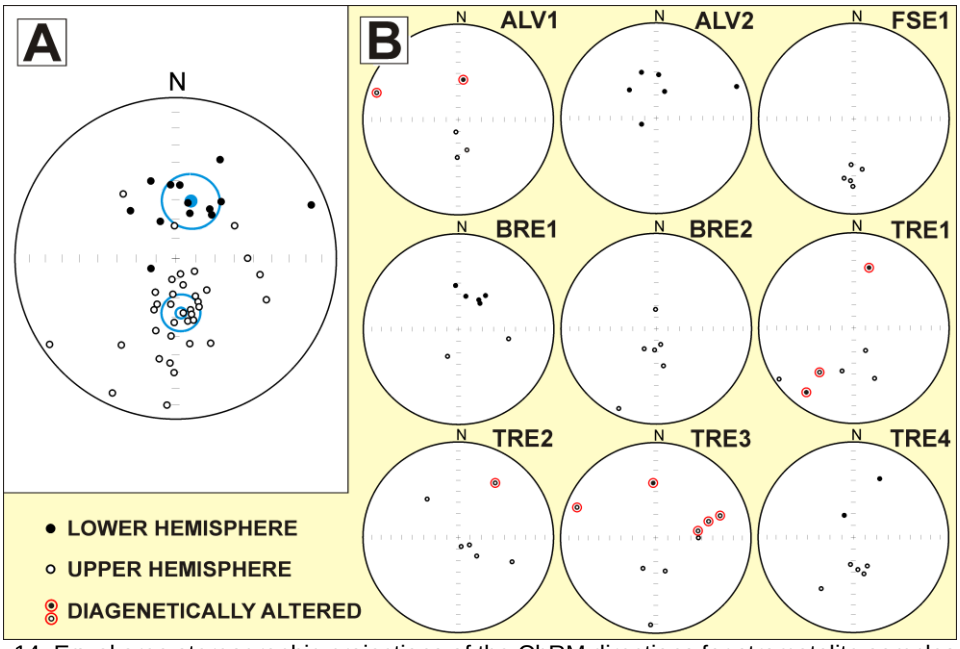

Fig. 14: Equal area stereographic projections of the ChRM directions for stromatolite samples. A: Directions for all samples, including means and 95% confidence areas of the normal-polarity and reversed-polarity populations. B: Directions for individual sites.

Regarding the samples showing signs of diagenetic alteration (Fig. 14B), they usually yield anomalous directions (e.g. most samples of site TRE3) that probably result from the overlapping of two or more stable components. In site TRE1B, which represents a highly calcitized stromatolite, several components are recognizable having both normal and reversed polarities, suggesting a complex diagenetic history. In site ALV-1, the only sample with normal polarity shows signs of moderate calcitization, therefore that polarity is tentatively interpreted as dominated by a diagenetic ChRM component.

4.4 U-series dates

To constrain the minimum age of the detrital sediments overlying the stromatolites, we present 19 new U-Th dates from three stalagmites and one flowstone that grew in the main relict canyon (Table 1). Stalagmite ORG2 (Fig. 4A) grew from ~485 to ~399 ka BP (Table 1) over sands covering stromatolite levels ST3 and ST4. Flowstone ECA8 yielded ages from ~486 to ~456 ka (Table 1). In both speleothems the uncertainties of the dates are relatively large (from ~12 to ~43 ka), mainly because the ages are close to the upper age limit of the U-Th disequilibrium method. Two of the dates of stalagmite ECA7, which grades laterally into flowstone ECA8, have very large errors due to analytical problems (higher U content than expected). The age (~401

ka) and error (~49ka) of one additional ECA7 date are comparable to the results of ECA8 and ORG2, indicating a period of significant speleothem growth from ~485 to ~400 ka in this area of the main relict canyon, postdating the deposition of sand that in turn postdated the stromatolites (Fig. 4A). Stalagmite SIR1 also grew over sand deposits overlying stromatolites (ST4: Fig. 7A) from ~78.9 to ~8.1 ka BP.

Sample ID	**Stalag**	mm from top	Mineral	**[230Th /238U]**	±95%	**[234U/ 238U]**	±95%	**[232Th/ 238U]**	±95%	**[230Th/ 232Th]**	**U-Th Age Ka**	±95%	**[234U/238U]i**	±95%
ORG2E-U	**ORG2**	7	Calcite	1.8321	0.0074	1.6460	0.0031	0.00051	0.000014	3595.1	**399.63**	12.186	**3.001**	0.0649
ORG2E-S	**ORG2**	345	Calcite	2.2059	0.0079	1.8828	0.0039	0.00166	0.000020	1328.4	**485.17**	19.860	**4.480**	0.1875
ECA8C-Z	**ECA8**	23	Calcite	1.1187	0.0058	1.0981	0.0021	0.00015	0.000001	7390.7	**457.70**	35.362	**1.358**	0.0333
ECA8C-Y	**ECA8**	27	Aragonite	1.0860	0.0049	1.0710	0.0022	0.00002	0.000003	65502.7	**485.96**	43.005	**1.281**	0.0312
ECA7D-Q	**ECA7**	53	Calcite	1.0998	0.0140	1.0756	0.0023	0.00004	0.000002	24692.8	**569.24**	*216.2*	**1.402**	0.4301
ECA7D-P	**ECA7**	246	Calcite	1.0749	0.0134	1.0759	0.0021	0.00009	0.000004	11440.2	**401.05**	49.37	**1.236**	0.0331
ECA7D-R	**ECA7**	437	Calcite	1.0481	0.0159	1.0504	0.0038	0.00002	0.000013	46095.7	**434.68**	97.12	**1.174**	0.0542
SIR1D-AA	**SIR1**	5	Calcite	0.0987	0.0025	1.3443	0.0061	0.00127	0.000036	78.0	**8.135**	0.267	**1.351**	0.0063
SIR-1-35	**SIR1**	57	Calcite	0.1193	0.0023	1.3287	0.0041	0.00051	0.000010	235.9	**10.17**	0.217	**1.338**	0.0041
SIR-1-34	**SIR1**	129	Calcite	0.1174	0.0022	1.3459	0.0049	0.00025	0.000010	477.5	**9.90**	0.200	**1.356**	0.0049
SIR1D-AB	**SIR1**	181	Calcite	0.1256	0.0018	1.3454	0.0057	0.00038	0.000015	328.3	**10.59**	0.170	**1.355**	0.0058
SIR-1-33	**SIR1**	213	Calcite	0.1274	0.0018	1.3307	0.0037	0.00018	0.000029	711.0	**10.92**	0.166	**1.341**	0.0038
SIR-1-32	**SIR1**	256	Calcite	0.1370	0.0018	1.3377	0.0043	0.00025	0.000009	542.0	**11.72**	0.170	**1.349**	0.0044
SIR-1-31	**SIR1**	287	Calcite	0.1590	0.0029	1.3774	0.0067	0.00058	0.000009	272.2	**13.25**	0.276	**1.392**	0.0069
SIR-1-30	**SIR1**	333	Calcite	0.1707	0.0020	1.3560	0.0040	0.00037	0.000006	466.8	**14.56**	0.194	**1.371**	0.0042
SIR1D-AC	**SIR1**	338	Calcite	0.3707	0.0026	1.2985	0.0050	0.02103	0.000415	17.6	**33.48**	2.656	**1.327**	0.0059
SIR-1-29	**SIR1**	395	Calcite	0.4878	0.0060	1.2704	0.0032	0.00127	0.000022	383.9	**51.74**	0.843	**1.313**	0.0036
SIR-1-28	**SIR1**	464	Calcite	0.6247	0.0059	1.2401	0.0031	0.00063	0.000014	987.0	**74.35**	1.028	**1.296**	0.0037
SIR1D-AD	**SIR1**	523	Calcite	0.6593	0.0068	1.2523	0.0037	0.00075	0.000024	880.9	**78.89**	1.215	**1.314**	0.0044

Table 1: Uranium-series analyses of speleothems with U-Th disequilibrium from the main relict canyon of El Soplao (brackets denote activity ratios; i = initial). U-Th ages and [234U/238U]i were calculated assuming an initial [230Th/232Th] of 1.5±1.5. All uncertainties are two-sigma.

4.4.1 Recalculation of U-U ages of stalagmites with U-Th secular equilibrium

Stalagmites FS61, FS63 and COL1 also grew in the main relict canyon of El Soplao but they are in U-Th secular equilibrium (Rossi el al., 2010), implying they are older than ~500 ka. FS61 and FS63 overlie sand covering reversed-polarity ST2 stromatolites (FS site) (Fig. 3A). COL1 grew over a sandy sequence of unclear relationship to stromatolites, but is located at 513 m asl, broadly the same elevation of stromatolite ST1 in that area of the canyon (Fig. 4A). Flowstone sample SPL-00 (after Gázquez et al., 2014) is also in U-Th secular equilibrium and grew in the main relict canyon too, overlaying clastic sediments that in turn cover ST3 stromatolites (Fig. 3A). In the four speleothems (FS61, FS63, COL1 and SPL-00), 234U/238U activity ratios are above unity, hence their age can be calculated from the degree of U-U disequilibrium. However, for that calculation one needs to assume an initial 234U/238U activity ratio, which can only be determined directly in samples with U-Th disequilibrium. Based on data of two samples in U-Th disequilibrium from the main relict canyon (BO2, Fig. 4A), Rossi et al. (2010) calculated U-U ages for stalagmites FS61, FS63, and COL1 (0.95-0.98, 0.99, and 1.67 Ma ±0.25 Ma, respectively) assuming an initial 234U/238U ratio of 3 plus or minus a factor of two of the excess 234U.

That assumption and the resulting U-U ages can now be improved by using the new initial 234U/238U data of speleothems with U-Th disequilibrium reported here (Table 1). For the purposes of initial 234U/238U, stalagmite ECA7 and flowstone ECA8 are considered as a single site. Average initial 234U/238U activity ratios for the three speleothem sites with U-Th disequilibrium reported here are 3.74, 1.29, and 1.34 (Table 1), and 3.20 for stalagmite BO2 (Rossi et al. 2010). Besides, we have calculated initial 234U/238U ratios for three subsamples of flowstone SPL in U-Th disequilibrium based on data by Gázquez et al. (2014), resulting in a mean value of 1.33 for that flowstone. Therefore the average initial 234U/238U activity ratio for the five speleothems in U-Th disequilibrium is 2.39. These speleothems and also those in secular U-Th equilibrium grew in the same ~300-m-long area of the main relict canyon (Figs. 3A and 4A). By using that value (2.39) as an estimate of the initial 234U/238U activity ratio in drip waters prior to 500 ka in that area of the cave, plus or minus a factor of two of the excess 234U, U-U ages can be recalculated (or calculated) for FS61, FS63, COL-1 and SPL-00 (Table 2).

Given the relatively large range of assumed initial 234U/238U activity ratios (i.e. from 1.59 to 3.36), the uncertainty of the U-U ages is high (~245 ka), but still the ages are useful for the purposes of this study. Compared to the U-U ages of Rossi et al. (2010), the U-U ages calculated here are slightly younger (most around 0.8 Ma ± 0.25), but still the oldest age approaches 1.5 Ma.

speleothem	U-U age ka	± ka	assumed initital 234/238ai	minus half of the excess 234/238ai	plus half of the excess 234/238ai
COL-1	1490	245	2.18	1.59	3.36
FS63K	765	245	2.18	1.59	3.36
FS63M	798	245	2.18	1.59	3.36
FS61D	806	245	2.18	1.59	3.36
SPL00	783	245	2.18	1.59	3.36

Table 2: U-U ages. See text for explanation.

4.6 Sand composition and provenance

Samples POG-7 and PLY-1 are similar, dominated by quartz (84-77%), dolomite (8-11%), K-feldspar (0.4-3%), and iron-oxide grains (4-6%), with subordinate presence of sandstone rock fragments and stable heavy minerals. Quartz grains regularly show inherited overgrowths (sensu Rossi and Alaminos, 2014) and sandstone rock fragments are mostly of quartz- and kaolinite-cemented quartzarenites and subarkoses. The dolomite fragments are regularly highly corroded, showing abundant intracrystalline secondary porosity. The margins of dolomite grains are abraded and in cases rounded, commonly showing diagenetic calcite overgrowths. The regular presence of inherited quartz overgrowths, and the presence of quartz-cemented sandstone rock fragments, clearly indicates that the siliciclastic sand fraction is derived from the erosion of Triassic Buntsandstein sandstones. The Albian to Cenomanian sandstones of the Sierra de Arnero can be discarded as possible sand sources because the thermal maturity of those sandstones is too low (Najarro et al., 2009) to have quartz overgrowth cement. Sample POS-1, at the base of a normal-polarity argillaceous sequence (POL), is largely dominated by dolomite clasts (79%), with subordinate iron oxides (14%), quartz (6%), and K-feldspar (1%).

5. Discussion

5.1 Notches and stromatolites as paleo-water table indicators

Because the Arnero caves are developed in steeply-dipping strata, the low-gradient profiles of both notches and stromatolites strongly suggest that they formed in cave-stream subhorizontal passages at the water table. If the notches resulted from differential erosion of less resistant beds, they would be steeply inclined rather than subhorizontal. The regular presence of coarse siliciclastics interbedded within the stromatolites further supports that interpretation, since gravel tends to be deposited preferentially along water-table passages (e.g. Stock et al., 2005) rather than in phreatic passages where clay and silt predominate (Ford and Williams, 2007). It is very unlikely that the Arnero notches represent paragenetic solution ramps formed at sediment-water interfaces bellow the water table. Such interfaces are typically irregular or undulating, hence the resultant solution ramps also present that geometry (Farrant and Smart, 2011), rather than being persistently subhorizontal as the notches reported here. Although subhorizontal notches can also form in vadose cave passages floored by clastic sedimentation not controlled by the water table (Farrant and Smart, 2011), in the Arnero caves that possibility is unlikely because: (1) notches occur in virtually all the low-gradient canyons across the cave system; and (2) in the main relict canyon, several notches are stacked vertically and maintain their low gradients for long distances, features difficult to explain if the notches were graded to a local sediment of breakdown obstruction within the cave.

Probably the most unequivocal evidence supporting that the studied stromatolites and notches formed along ancient water tables is their relationship to relict vadose-phreatic transitions, i.e. the points where passage morphology changes from vadose to phreatic. Where such transitions

are not obscured by later erosion or sedimentation, their elevations define the position of the contemporary water tables, in cases rather precisely (e.g. Palmer, 1989; Häuselmann et al., 2007). In the main relict canyon, multiple vadose (or epiphreatic) to phreatic transitions occur at the same level of stromatolites and notches. In cases, the canyon ceiling descends below the elevation of the stromatolite/notch level, passing into a phreatic conduit devoid of notches or stromatolites (e.g. Fig. 3A, 4A). In other cases, a phreatic tube emerges from the canyon floor or wall at the same elevation as a stromatolite/notch level (e.g. Fig. 4A, 7A).

If the stromatolite levels and associated notches represent paleo-water tables, then projected elevations of these features will show the topography of the paleo-water table surfaces, allowing the analysis of their geometry. For that purpose, the assemblage defined by stromatolite levels ST1 to ST4 is probably the most useful because is the most continuous: it can be followed for more than 2 km across the cave system (Fig. 2B), defining a low relief surface with an overall slope of 1.7º to the east. This gradient is consistent with the present-day inferred relief of the water table, based on the altitude of the resurgence and the lowest elevation of the mine passages that were not flooded when the mine closed and water pumping ceased (Fig. 2B). Notably, very similar paleo-water table slopes have been defined in relict alpine cave systems by geomorphic mapping (~1.6°: Plan et al., 2009; 1.3-2.1º: Häuselmann et al. 2003), further supporting the paleo-water table interpretation. The gradient defined by ST1-ST4 is not uniform, alternating sections with higher and lower slopes (Fig. 2B). Notably, the higher slopes occur where the cave intersects the sulfide mineralization, such as the Isidra and Florida mineralized bodies (Fig. 2) where slopes reach 2.5º and 2.3º, respectively. That suggests that the mineralized bodies acted as minor hydrologic barriers resulting from the relatively high degree of cementation of the dolostone porosity by sulfides and associated gangue phases. Such barriers apparently induced minor local damming in the phreatic paleoaquifer, resulting in a paleo-water table with a stair-like geometry.

5.2 Origin of the notches and speleogenetic implications

In the Arnero caves, at least three mechanisms, not mutually exclusive, can explain the formation of notches at paleo-water tables: (1) covering canyon floors with relatively insoluble materials may shield the bedrock floor against erosion thus favoring lateral dissolution; (2) enhanced mechanical erosion (corrasion) of canyon walls, related to transport of abrasive clasts along canyon floors; and (3) enhanced chemical erosion at the water table linked to acidity-generating reactions operating at water-cave atmosphere interfaces.

The first mechanism is likely of prime importance, since the Arnero notches are regularly associated with siliciclastics and ferromanganese deposits, both of which can protect canyon floors from chemical and physical erosion. The notches described here are thus comparable to alluvial notches (Farrant and Smart, 2011) but, in Arnero, the stromatolites played an additional mayor role in preventing erosion of passage floors.

The second mechanism (enhanced lateral mechanical erosion) could have also been significant in the Arnero caves. The clastic sediments interbedded with the stromatolites are highly abrasive: pebbles are predominantly quartzite, and the sand fraction is dominated by quartz. Moreover, the dolostone exposed on cave walls is commonly friable, hence particularly prone to mechanical erosion. However, the most compelling evidence for mechanical erosion is the presence of abraded dolomite grains in the sand fraction of the clastic sediments, implying that cave streams mechanically eroded the dolostone bedrock. The dolomite clasts also show signs of intense micro-scale corrosion, which probably occurred prior to corrasion or during stream transport.

The third possible notch-forming mechanism (enhanced chemical erosion) deserves special attention. The Arnero stromatolites mainly resulted from microbial oxidation of aqueous Mn(II) to MnO_2 (Rossi et al., 2010), a reaction that generates significant acidity (e.g.: $Mn^{2+} + ½O_2 + H_2O \Rightarrow MnO_2 + 2H^+$; Nealson, 2006). The same applies to the oxidation of aqueous Fe(II) to Fe(III) oxy-hydroxides, which are also present in the Arnero stromatolites (Rossi et al., 2010). To keep the pH within the stability limits of MnO_2, that acidity needs to be neutralized. Obviously, in the Arnero caves the easiest way to achieve that is by dissolving the carbonate host-rock. Given the

relatively high volumes of Mn oxides preserved in the Arnero stromatolites, significant volumes of dolostone were likely dissolved along passage walls, but not on passage floors which were covered by the stromatolites themselves. Therefore, enhanced lateral bedrock corrosion induced by manganese (and iron) oxidation seems a plausible mechanism to contribute to notch formation in Arnero caves.

The acidity generated by microbial Mn oxidation can be considered a mechanism of hypogenic speleogenesis, since the aggressiveness is produced underground rather than at the earth surface (Klimchouk, 2009). That process is comparable to the oxidation of Fe^{2+} released by the dissolution of Fe carbonates producing acidity (Kempe, 2014). Although the acidity generated by microbial oxidation of Mn has previously been invoked as a potential agent for small-scale dissolution of cave walls (Northup et al., 2000), to our knowledge that mechanism has not been considered as a significant speleogenetic mechanism so far.

To date, we have not observed stromatolites in phreatic ramps. The most obvious explanation of the absence of stromatolites in phreatic conduits is that stromatolites only formed at the water table. In fact, this surface is the ideal locus for Mn(II) oxidation. In nature, dissolved Mn(II) and Fe(II) are only significant in waters depleted in O_2, therefore it is likely that the Arnero paleo-cave streams were partly fed by O_2-depleted phreatic waters. This is not a problem in Arnero, where the oxidation of sulfide bodies undoubtedly consumed much oxygen. Upon reaching the low-gradient cave streams, the relatively O_2-poor and Mn(II)-rich waters interacted with the O_2-rich cave atmosphere, promoting Mn oxidation at the water table.

5.3 Epigenic versus hypogenic speleogenesis

The erosional meso-morphology of most passage walls in Arnero caves is rather distinctive: rough and irregular, commonly rounded forms (Fig. 6), spongeworks (Fig. 9C), friable halos, and absence of scallops. This contrasts with the smoother, more regular, and commonly scalloped morphologies typical of epigenic limestone-cave passage walls.

The characteristic rockwall morphology of Arnero caves resembles that of hypogenic caves, which also typically develop rounded ceiling forms, spongeworks, wall and ceiling half-tubes (Klimchouk, 2009), corrosion notches (De Waele et al., 2014), and halos of weathered walls linked to condensation-corrosion (Auler and Smart, 2003). Additional features suggesting hypogenic speleogenesis are the relatively large size of the Arnero caves compared to the limited outcrop surface of the Reocín Formation (Fig. 1C) and the paucity of natural hydrologically active entrances to Arnero caves. However, the characteristic erosional morphologies can be explained without invoking hypogenic or condensation-corrosion processes (section 5.4) and some features of Arnero caves do not match a model of purely hypogenic speleogenesis. First, the abundance of allogenic sediment points to important inputs of surface-derived waters. Pebble and sand composition indicates that much of that sediment was supplied by surface streams draining outcrops of Triassic Buntsandstein, similar to what is happening today in La Cuerre sink (Fig. 1C). The drainage area of the Arnero caves was likely much larger before: as erosion progressed, streams draining Triassic outcrops have been progressively captured by tributaries of the Nansa and Bustriguado rivers, preventing those streams from contacting the Reocín carbonates (Fig. 1C). The higher past allogenic recharge explains the relatively large size of the relict Arnero caves compared to their present-day drainage area. Second, the conduit pattern of Arnero caves (trunk passage with inlets, absence of mazes) is more consistent with epigenic rather than hypogenic speleogenesis (Klimchouk, 2009).

Still, a hypogenic contribution related to sulfuric acid produced by oxidation of iron disulfide (e.g. Auler and Smart, 2003; Tisato et al., 2012) is plausible for the Arnero caves. This is because the volumetrically important Pb-Zn sulfide deposits intersected by the caves contain some pyrite and marcasite. Actually, the local presence of melanterite adjacent to pyrite in mine galleries evidences that sulfuric acid is being produced today by pyrite oxidation. Besides, in the uppermost ~150 m of the mineralized bodies, Pb-Zn sulfides are largely oxidized and transformed into higher-grade carbonates and silicates—the main target of initial mining. Undoubtedly, sulfuric acid was generated by the oxidation of the FeS_2 originally present in the

supergene zone, which must have contributed to speleogenesis in Arnero. Nevertheless such contribution is probably subordinate given the absence of extensive gypsum deposits, the subordinate amounts of FeS_2 in sulfide bodies, and the evidences of allogenic recharge into the caves.

5.4 Origin of the irregular erosional wallrock morphologies

Particularly in the western sector of the cave system, many of the rounded forms protruding from cave walls and ceilings clearly represent pendants and half tubes, i.e. paragenetic features formed by phreatic dissolution in passages almost completely filled with sediments (Lauritzen and Lundberg, 2000) (Fig. 3F, 5A, 6). Even where the rounded protuberances do not resemble typical pendants, clay and silt is frequently present between the irregular forms, indicating an origin related to paragenesis rather than condensation-corrosion.

Apart from paragenesis, the porous nature of the host dolostone can adequately explain most of the irregular rockwall morphologies of Arnero caves, including spongeworks and friable halos. Remarkably, the rare passages developed in limestone do not show the spongeworks or irregular forms observed in dolostone walls. Instead, limestone walls show regular and smooth surfaces (Fig. 9B), and well developed scallops in canyon passages (Fig 9D). On surface outcrop the different morphologies of dolostone and limestone are also apparent, with spongeworks limited to dolostone. Therefore, the different morphologies are related to lithology, with dolostone walls resulting in irregular forms and spongeworks. Rather than differences in mineralogy, the cause of the different behaviors of dolostone and limestone is their matrix porosity: negligible in the Reocín limestones, significant in the Reocín dolostones.

Because of the increased surface area related to the matrix porosity in the dolostone, dissolution may occur adjacent to the walls of hydrologically active conduits. This can explain the halos of enhanced intercrystalline solutional porosity in the walls of Arnero caves. The distribution of porosity in the dolostone is irregular and commonly vuggy. Such irregular distribution of porosity and thus of permeability will promote irregular dissolution, explaining the spongeworks observed in both underground and surface dolostone outcrops. In fact, spongework is typical of caves developed in geologically young limestones because they have significant matrix porosity (Palmer, 1991; Florea, 2006, Moore, 2009; Ginés et al., 2014). In the Arnero case, the Aptian dolostone retains matrix porosity despite not being geologically young, while the coeval limestones show negligible matrix porosity. Such contrast reflects the fact that dolostones are usually more porous than limestones, because the former are less prone to mechanical and chemical compaction and thus to burial porosity loss. In the Arnero caves, the presence of matrix porosity in the dolostone explains not only its peculiar erosional forms, but also the paradox that virtually all cave development in Arnero is focused on the dolostone while dolomite is much less soluble than calcite.

An additional effect than can contribute to explain the irregular dolostone wallrock forms is mechanical erosion. The increase in intercrystalline porosity in the dolostone exposed on cave walls results in a friable halo prone to mechanical erosion, particularly where abrasive clasts are transported by the cave streams (as discussed in section 5.2). Actually, this mechanism is apparently the main cause of the irregular solution pockets and spongework recorded in Florida caves receiving allogenic recharge, in which friable solutional halos develop on cave walls and are irregularly eroded by sediment-laden waters circulating through the conduits (Moore, 2009).

5.5 Impact of allogenic sediment influx on the development of water-table passages

In the Arnero relict caves, water-table canyons predominate to the west, while looping phreatic conduits prevail to the east, i.e. in the paleo-downstream direction. In particular, during ST1-ST5 time, the main water-table canyon passed in the downstream direction into a system of predominantly phreatic conduits. This distribution is apparently unrelated to changes in the geological structure, which is relatively simple and dictates dominance of strike-oriented flow (Fig. 1C). Actually, most cave passages in Arnero are developed along bedding planes. This flow configuration should favor the development of water-table passages, because the portions

of bedding planes closer to the water table represent very efficient and direct flow paths (Palmer 1991). Still, looping phreatic conduits are dominant downstream, indicating that the direction of flow relative to the strike was not a key factor controlling the water-table versus phreatic development in this case. Changes in fissure frequency (Ford and Williams, 2007) do not seem to be a major control either, given the simple geological structure. Other factors that can control water-table versus phreatic development, such as floodwater variations or the history of base level lowering (Gabrosek et al., 2014) better explain temporal changes in passage distribution rather than lateral, coeval changes.

In Arnero, the input of allogenic sediments offers a plausible explanation for the observed trend of changing from water-table canyons to phreatic loops in the paleo-downstream direction. Clastic sediments and paragenetic morphologies are much more abundant in the paleo-upstream sector of the cave system, becoming scarce downstream, indicating that the sediment source (i.e. allogenic streams draining off Buntsandstein outcrops) was located to the west, i.e. similar to the present-day configuration (Fig. 1C). The input of allogenic sediments favored water-table passages in the upstream sections because sediment filling of phreatic conduits favors water-table drainage by inducing bypassing of sediment-filled loops (Ford and Williams, 2007). In addition, sediment filling of canyon floors prevents the development phreatic undercaptures during episodes of base-level lowering, thus favoring notched water-table canyons (Farrant and Smart, 2011). Actually, water-table cave passages are common in nearby areas of the Cantabrian Mountains where allogenic streams draining Triassic Buntsandstein enter the caves (e.g. Torca Labarga: Smart, 1986; Cobre Cave: Rossi et al., 2014), further supporting a relationship between allogenic sediment input and water-table caves.

5.6 Age of the paleo-water tables

The U-series ages of stalagmites and flowstones from the main relict canyon provide minimum estimates of when that canyon became vadose. The basal ages of speleothems with U-Th disequilibrium range from ~485 to ~80 ka, indicating that the main relict canyon remained in the vadose zone for at least the last ~0.5 Ma. The basal date of stalagmite ORG2 indicates that the sand overlying stromatolites ST3-ST4 is at least ~485 ±20 ka old. Stalagmite SIR1 also grew over sand postdating ST4 stromatolites, but its basal date is relatively young (78.9 ±1.3 ka); therefore the basal ORG2 date provides a better minimum estimate of the age of the sand overlying the stromatolites.

The speleothems with U-Th secular equilibrium provide much better minimum estimates of the age of the main relict canyon and its deposits. Three of these speleothems overlie sands that in turn cover stromatolites ST2 and ST3, and have yielded similar U-U ages (0.80 ±0.25 Ma, 0.81 ±0.25 Ma, and 0.78 ±0.25 Ma) indicating that the stromatolites and associated sands are at least ~0.80 ±0.25 Ma old. Again, this is only a minimum estimate, since the abandonment of this passage by phreatic waters and the subsequent formation of the stromatolites at the water table could have happened earlier.

The oldest U-U age (1.49±0.25 Ma) is from a stalagmite (COL1) whose relationship to the stromatolites is unclear, but it grew in the main relict canyon. This ~40-cm-long aragonite stalagmite is devoid of detrital material, suggesting that the passage was already hydrologically inactive when it precipitated. Therefore the main relict canyon transformed into a vadose passage prior to ~1.5 Ma (±0.25 Ma). Since COL1 grew at the same elevation as ST1, that is probably the minimum age of this stromatolite level and the corresponding paleo-water table.

The clay and silt predating ST1-ST4 stromatolites regularly show reversed polarities; therefore they are older than the Brunhes-Matuyama reversal at 0.78 Ma. Most stromatolite samples from ST1 to ST4 also show reversed polarities, therefore their minimum age is 0.78 Ma too. Siltstone postdating ST4 also shows reversed polarity, further supporting that view. This is consistent with the U-U ages of speleothems postdating those stromatolites, which are about 0.8 Ma (± 0.25). Again, these are minimum ages for the stromatolites. Assuming that the reversed-polarity stromatolites formed during the Matuyama Chron, their true age could be as old as 2.6 Ma. Assigning the reversed-polarity sediments and stromatolites to other, pre-Matuyama reversed period is possible but probably unlikely: it would imply stromatolite ages older than ~3 Ma,

resulting in mean rates of base-level lowering probably too low (<100 m per Ma) for an alpine setting. Therefore the stromatolites most likely formed during the Matuyama Chron.

The presence of two stromatolite sites (BRE-1, TRE-4) with both normal and reversed polarities in apparently unaltered samples suggests that the normal polarities could correspond to the Jaramillo (~0.99-1.07 Ma) and/or Olduvai (~1.77-1.96 Ma) sub-Chrons. However, at present we cannot completely rule out a diagenetic origin for the normal polarities. However, other stromatolite samples with obvious diagenetic alteration typically show more than one stable paleomagnetic component and anomalous paleomagnetic directions. This is not the case for the normal-polarity samples of BRE-1 and TRE-4, suggesting that these normal polarities are depositional.

Given that the ST1-ST4 stromatolites formed during the Matuyama Chron, and that the oldest U-U speleothem date in the low-gradient canyon is ~1.5 Ma (+-0.25), then those stromatolites must have formed at some point during the lower part of the Matuyama, i.e. from ~1.5 Ma (+-0.25) to ~2.6 Ma. Therefore, if the normal polarities recorded by BRE-1 and TRE-4 are depositional, they probably represent the Olduvai sub-Chron.

Below the level of stromatolite ST4, all the analyzed samples show normal polarities, including stromatolite ST5 (ALV2 site) and clays and silts (POL site) correlative to ST10. This configuration suggests that the Brunhes-Matuyama boundary could be located between ST4 and ST5. However, due to our limited sampling below ST5, and to the inherent limitations of magnetostratigraphy when applied to cave deposits (e.g. Sasowsky et al., 1995), it remains unclear if the ALV2 and POL sites represent the Brunhes or an older normal sub-Chron.

In summary, the available data indicates that the stromatolites of the main relict canyon ST1 to ST4 formed during the Matuyama Chron, most likely prior to ~1.5 Ma (+-0.25). Stromatolite level ST5 and clastic sediments correlative to ST10 show normal polarities, suggesting that they could have formed during the Brunhes Chron (i.e. after 0.78 Ma).

The inferred present-day water table is located ~320 m below the level of the ST1-ST4 stromatolites. Although no present-day water-table cave passages have been explored yet in Arnero, the location of the water table can be inferred by extrapolating a ~1.7º slope from the current resurgence location. The resultant water table is in good agreement with the constraints provided by elevations of unflooded mine passages (Fig. 2B). Therefore, the water table has fallen ~320 m since the formation of stromatolites ST1-ST4. Taking into account the U-U and paleomagnetic age constrains, which indicate that those levels likely formed during the Matuyama Chron but prior to ~1.5 Ma, the resultant long-term rate of base level lowering ranges from ~125 to ~213 m per Ma. These are probably reasonable figures for a moderate altitude Alpine setting (Häuselmann et al., 2007), but significantly higher that those typical of more stable continental regions (~60-30 m/Ma: Sasowsky et al., 1995; Granger et al., 2001). In the nearby Picos de Europa karst massif, which is located only ~20 km to the west of Arnero, Smart (1986) deduced a long-term rate of base level lowering of ~ 300 m per Ma, i.e. faster that those deduced in Arnero. Being based on vadose speleothem U-Th dates, that figure was a maximum estimate, hence consistent with the Arnero values.

Unlike other cave deposits, which may be much younger that the hosting passage, the Mn-stromatolites considered here arguably formed when the passage was at the water table. Therefore Mn-stromatolites may be particularly useful to define and date paleo-water tables, comparable to the case of other rare spleothems that also form at o near water tables such as cave mammillaries (Polyak et al., 2008), or certain raft calcites (Piccini et al., 2015). To date, cave Mn deposits interpreted as unequivocal stromatolites have only been described in Arnero caves (El Soplao: Rossi et al. 2010; Juñoso: this article). However, cave stromatolites in general are probably more common than previously thought (e.g. Lundberg and McFarlane, 2011). In particular, ferromanganese stromatolites are expected to form preferentially in caves developed in dolostone, where dolomite dissolution can supply significant Mn(II). For instance, the Rescaño Cave (Udías, Cantabrian Mountains: Fig. 1B) contain Mn stromatolite levels similar to those in Arnero (unpublished data), and the relatively thick ferromanganese deposits reported in some American (White et al., 2009) and European caves (Onac, 1996; Onac et al., 1997) probably represent water-table stromatolites too.

Conclusions

The stromatolites and subhorizontal notches of Arnero relict caves formed in cave-stream passages at the water table. The best-defined paleo-water tables show an overall slope of 1.7º, consistent with the present-day inferred relief of the water table, with segments of higher slope where the cave intersects minor hydrological barriers related to sulfide mineralization.

The formation of ferromanganese stromatolites at the water table induces wall notching by the combined effect of enhanced acidity by Mn-Fe oxidation and shielding of cave floors against erosion by the stromatolites themselves. Besides, abrasive clastic sediments contributed to notch formation by protecting passage floors from dissolution and especially by promoting mechanical erosion of cave walls.

The genesis of the Arnero relict caves is dominantly epigenetic, consistent with the conduit pattern and the abundant allogenic sediments. The observed trend of changing from water-table canyons to phreatic loops in the paleo-downstream direction is related to the upstream input of allogenic sediments, which favored upstream water-table passages by inducing bypassing of sediment-filled loops and preventing the development phreatic undercaptures during episodes of base-level lowering. The relatively large size of the relict Arnero caves compared to the present-day outcrop area of the hosting carbonates is linked to a decrease in the drainage area of allogenic streams. However, at least two hypogenic processes (in a geochemical sense) contributed to speleogenesis: Mn-Fe oxidation at water tables and FeS_2 oxidation in the sulfide-filled paleocave systems intersected by the Arnero caves.

The irregular wallrock erosional forms of Arnero caves are related partly to paragenesis and partly to the presence of matrix porosity in the host dolostones. Similar to immature limestones, the dolostone matrix porosity favored intercrystalline irregular dissolution near passage walls, generating friable halos. Subsequent mechanical erosion further contributed to generate the irregular rounded forms and spongeworks. The dolostone porosity also explains the paradox that virtually all cave development in Arnero is focused on dolostone despite being much less soluble than adjacent limestone

U-series dating of carbonate speleothems and paleomagnetic data from ferromanganese stromatolites and clastic sediments indicate that the paleo-water tables recorded ~320 m above the present-day water table formed during the lower part of the Matuyama Chron, most likely prior to ~1.5 Ma (+-0.25 Ma), implying a long-term rate of base level lowering ranging from ~125 to ~213 m per Ma.

Cave stromatolites are excellent geomagnetic recorders, suitable for paleomagnetic dating. Similar of other spleothems that also form at or near water tables, ferromanganese stromatolites offers a direct way to define and date paleo-water tables, especially in caves developed in dolostone, therefore they are potentially useful to study the evolution of landscapes.

Acknowledgements

Financial support was provided by grants ICT-Soplao-53.5.00.12.00 (IGME - provincial government of Cantabria - Turismo del Nansa) and CGL2012-38481 (Ministerio de Economía y Competitividad - European Regional Development Fund). We thank A. Argumosa (El Soplao SL) for greatly facilitating our research in the cave, X. Perrier for guiding us through the most remote areas of the caves and for rigging most of the vertical sections, and S. Torres, N. Isanta, E. Camuñas, S. Menéndez, M. Tudela, A. Uyarra, and E. Baeza for their fieldwork assistance.

References

Álvarez-Marrón, J. Rubio, E. Torne, M., 1997. Alpine age subduction structures in the North Iberian Margin. Journal of Geophysical Research 102, 22495–22511.

Auler, A.S., Smart, P.L., 2003. The influence of bedrock-derived acidity in the development of surface and underground karst evidence from the Precambrian carbonates of semi-arid northeastern Brazil. Earth Surface Processes and Landforms 28, 157–168.

De Waele, J., Plan, L., Audra, P., Vattano M., and Madonia G., 2014, Sulfuric acid water table caves (Grotte du Chat / Acqua Fitusa /Bad Deutsch Altenburg + Kraushöhle). Karst Waters Institute special publication 18, 31-35.

Delgado Huertas, A., Forti, P., Stöll, H. and Calaforra. J.M., 2010. Variabilidad paleoambiental de la Cueva de El Soplao (Cantabria) a partir de la diversidad mineralógica de sus espeleotemas. In: J.J. Durán and F. Carrasco (Eds.), Cuevas: Patrimonio, Naturaleza, Cultura y Turismo. Asociación de Cuevas Turísticas Espanolas, Madrid. 393-304.

Farrant, A.R., Smart, P.L., 2011. Role of sediment in speleogenesis; sedimentation and paragenesis. Geomorphology 134, 79–93.

Farrant, A.R., Smart, P.L., Whitaker, F.F., Tarling, D.H., 1995. Long-term Quaternary uplift rates inferred from limestone caves in Sarawak, Malaysia. Geology 23, 357–360.

Florea L.J., 2006, Architecture of air-filled caves within the karst of the Brooksville Ridge, west-central Florida. Journal of Cave and Karst Studies 68, 64–75.

Ford, D.C., Williams, P., 2007. Karst hydrogeology and geomorphology. Wiley, Chichester, UK. 562 pp.

García, G., Palero, F.J., Rabadán, J., Medrosa, M., 2007, La Florida. *Bocamina* 20, 14-79.

Gabrovšek, F. Häuselmann, P., Audra P., 2014. 'Looping caves' versus 'water table caves': the role of base-level changes and recharge variations in cave development. Geomorphology 204, 683-691.

Gázquez F., Calaforra J.M, Rull F., Forti P., García-Casco A., 2012. Organic matter of fossil origin in the amberine speleothems from El Soplao Cave (Cantabria. Northern Spain). International Journal of Speleology 41, 113–123.

Gázquez, F. Calaforra, J.M. Forti, P. Stoll, H. Ghaleb, B. Delgado-Huertas, A., 2014. Paleoflood events recorded by speleothems in caves. Earth Surf. Process. Landforms 39, 1345–1353.

Ginés J., Fornós J.J., Ginés A., Merino A. and Gràcia F., 2014. Geologic constraints and speleogenesis of Cova des Pas de Vallgornera, a complex coastal cave from Mallorca Island (Western Mediterranean). International Journal of Speleology 43, 105-124.

González, M., 2011, De las primeras exploraciones a la topografía 3-D. En: El Soplao, una ventana a la ciencia subterránea. Gobierno de Cantabria, Consejería de Cultura, Turismo y Deporte, p. 106-109.

Granger, D.E., Fabel, D., and Palmer, A.N., 2001, Pliocene-Pleistocene incision of the Green River, Kentucky, determined from radioactive decay of cosmogenic 26Al and 10Be in Mammoth Cave sediments: Geological Society of America Bulletin 113, 825–826.

Häuselmann, P., Granger, D.E., Jeannin, P.-Y., Lauritzen S.-E. 2007. Abrupt glacial valley incision at 0.8 Ma dated from cave deposits in Switzerland. Geology 35, 143-146.

Häuselmann, P., Jeannin, P.Y., Monbaron, M., 2003. Role of epiphreatic flow and soutirages in conduit morphogenesis: the Bärenschacht example (BE, Switzerland). Zeitschrift fur Geomorphologie 47, 171–190.

Hellstrom, J.C., 2003, Rapid and accurate U/Th dating using parallel ion-counting multi-collector ICP-MS. Journal of Analytical Atomic Spectrometry 18, 1346-1351.

Kempe, S., 2014. Hypogene limestone caves in Germany: geochemical background and regionality. Karst Waters Institute special publication 18, 48-56.

Klimchouk, A.B., 2009. Morphogenesis of hypogenic caves. Geomorphology 106, 100-117.

Lauritzen, S.E., Lundberg, J., 2000. Solutional and erosional morphology of caves. In: Klimchouk, A., Ford, D.C., Palmer, A.N., Dreybrodt, W. (Eds.), Speleogenesis: Evolution of Karst Aquifers. National Speleological Society, Huntsville, pp. 408–426.

Lowrie, W., 1990. Identification of ferromagnetic minerals in a rock by coercivity and unblocking temperature properties. Geophys. Res. Lett. 17, 159–162.

Lozano, R.P., Rossi, C., 2012. Exceptional preservation of Mn-oxidizing microbes in cave stromatolites (El Soplao, Spain). Sedimentary Geology 255-256, 42-55.

Lozano, R.P., Rossi, C., La Iglesia, A., Matesanz, E., 2012. Zaccagnaite-3R, a new Zn-Al hydrotalcite polytype from El Soplao cave (Cantabria, Spain). American Mineralogist 97, 513–523.

Ludwig, K.R., 1999, Berkeley Geochron. Center Spec. Pub., 2, 47.

Lundberg, J., McFarlane, D.A., 2011. Subaerial freshwater phosphatic stromatolites in Deer Cave, Sarawak - A unique geobiological cave formation. Geomorphology 128, 57-72.

McFadden, P.L., McElhinny, M.W., 1990. Classification of the reversal test in palaeomagnetism. Geophys. J. Int. 103, 725–729.

Meléndez, M. and Rodríguez, M.L., 2011. El agua subterránea, eterna protagonista: el acuífero de la Florida. En: El Soplao una ventana a la ciencia subterránea. Gobierno de Cantabria, p. 90-93.

Moore P.J., 2009, Controls on the veneration of secondary porosity in eogenetic karst: Examples from San Salvador Island, Bahamas and north-central Florida [Ph.D. thesis]: Gainesville, University of Florida, 140 p.

Najarro, M. Peñalver, E. Rosales, I. Pérez-de la Fuente, R. Daviero-Gomez, V. Gomez, B. Delclòs, X. 2009, Unusual concentration of Early Albian arthropod-bearing amber in the Basque-Cantabrian Basin (El Soplao, Cantabria, Northern Spain): Palaeoenvironmental and palaeobiological implications. Geologica Acta 7, 363–387.

Najarro M., Rosales I., Martín-Chivelet J., 2011. Major palaeoenvironmental perturbation in an Early Aptian carbonate platform: prelude of the Oceanic Anoxic Event 1a? Sedimentary Geology 235, 50–71.

Nealson, K.H., 2006, The Manganese-Oxidizing Bacteria. In: The Prokaryotes. Springer New York. 222–231.

Northup, D.E., Dahm, C.N., Melium, L.A., Spilde, M.N., Crossey, L.J., Lavoie, K.H., Mallory, L.M., Boston, P.J., Cunningham, K.I., Barns, S.M., 2000. Evidence for geomicrobiological interactions in Guadalupe Caves. Journal of Cave and Karst Studies 62-2, 80-90.

Onac, B.P., 1996. Mineralogy of speleothems from caves in the Padurea Craiului Mountains (Romania), and their palaeoclimatic significance. Cave and Karst Science 23, 109-124.

Onac B.P., Pedersen R.B., Tysseland M., 1997. Presence of rare-earth elements in black ferromanganese coatings from Vântului Cave (Romania). Journal of Cave and Karst Studies 59, 128–131.

Palmer, A.N., 1989. Geomorphic history of the Mammoth Cave System, in White, W.B. & White, E.L. (eds.), Karst hydrology; concepts from the Mammoth Cave area. New York, Van Nostrand Reinhold, p. 317–327.

Palmer A.N., 1991. Origin and morphology of limestone caves. Geological Society of America Bulletin 103, 1–21.

Plan, L. Filipponi, M. Behm, M. Seebacher, R. Jeutter, P., 2009. Constraints on alpine speleogenesis from cave morphology — A case study from the eastern Totes Gebirge (Northern Calcareous Alps, Austria). Geomorphology 106, 118–129.

Piccini, L. DeWaele, J. Galli, E.Polyak, V.J. Bernasconi, S.M. Asmerom Y., 2015. Sulphuric acid speleogenesis and landscape evolution: Montecchio cave, Albegna river valley (Southern Tuscany, Italy). Geomorphology 229, 134–143.

Polyak, V. Hill, C. Asmerom Y., 2008. Age and Evolution of the Grand Canyon Revealed by U-Pb Dating of Water Table-Type Speleothems. Science 319, 1377–1380.

Rossi, C., 2004. Picos de Europa, Spain. Encyclopaedia of Caves and Karst Science. Fitzroy Dearborn, New York-London, 582-585.

Rossi, C., Lozano, R.P. Isanta, N. and Hellstrom J. (2010): Manganese stromatolites in caves: El Soplao (Cantabria, Spain). Geology 38, 1119-1122.

Rossi, C., Mertz-Kraus, R. & Osete, M.L., 2014, Paleoclimate variability during the Blake geomagnetic excursion (MIS 5d) deduced from a speleothem record. Quaternary Science Reviews 102, 166-180.

Rossi, C. & Alaminos, A. 2014, Evaluating the mechanical compaction of quartzarenites: The importance of sorting (Llanos foreland basin, Colombia). Marine and Petroleum Geology, Volume 56, September, Pages 222-238.

Sasowsky, I.D., Schmidt, V.A., and White, W.B., 1995, Determination of stream-incision rate in the Appalachian plateaus by using cave sediment magnetostratigraphy. Geology 23, 415–418.

Serrano, E. González-Trueba, J.J. Pellitero, R. González-García, M. Gómez-Lende., M., 2013. Quaternary glacial evolution in the Central Cantabrian Mountains (Northern Spain). Geomorphology 196, 65–82.

Smart, P.L., 1986, Origin and development of glacio-karst closed depressions in the Picos de Europa, Spain: Zeitschrift fur Geomorphologie 30, 423–443.

Stock, G.M., Anderson, R.S., Finkel, R.C., 2004. Pace of landscape evolution in the Sierra Nevada, California, revealed by cosmogenic dating of cave sediments. Geology 32, 193–196.

Stock, G.M., Granger, D.E., Sasowsky, I.D., Anderson, R.S., Finkel, R.C., 2005. Comparison of U–Th, paleomagnetism, and cosmogenic burial methods for dating caves: implications for landscape evolution studies. Earth Planet. Sci. Lett. 236, 388–403.

Tavani, S. 2012, Plate kinematics in the Cantabrian domain of the Pyrenean orogen. Solid Earth 3, 265–292

Tisato N., Sauro F., Bernasconi S.M., Bruijn R., De Waele J. 2012. Hypogenic contribution to speleogenesis in a predominant epigenic karst system: a case study from the Venetian Alps, Italy. Geomorphology 151-152: 156-163.

Tornos F, Velasco F. 2011. Un yacimiento mineral muy especial. In: El Soplao: una ventana a la ciencia subterránea. Gobierno de Cantabria, p. 54–68.

White, W.B., Vito, C., Scheetz, B.E., 2009. The mineralogy and trace elements chemistry of black manganese oxide deposits from caves. Journal of Cave and Karst Studies 71, 136–143.